Volume 59
Number 40
18 May 2023
Pages 5933–6098

ChemComm

Chemical Communications

rsc.li/chemcomm

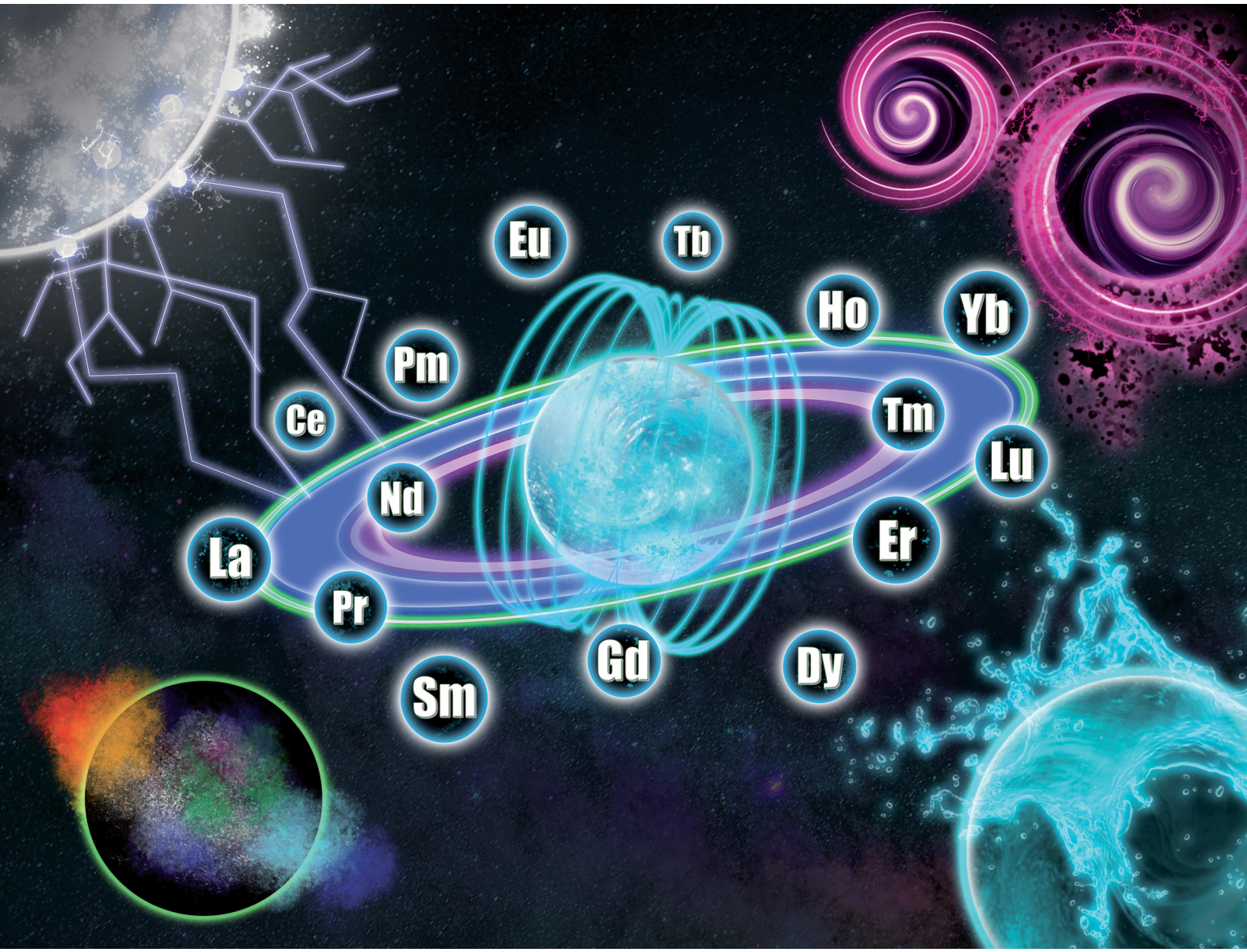

ISSN 1359-7345

ROYAL SOCIETY OF CHEMISTRY

FEATURE ARTICLE

Szymon Chorazy *et al.*

Multifunctionality of luminescent molecular nanomagnets based on lanthanide complexes

ChemComm

FEATURE ARTICLE

View Article Online
View Journal | View Issue

Cite this: *Chem. Commun.*, 2023, **59**, 5961

Multifunctionality of luminescent molecular nanomagnets based on lanthanide complexes

Robert Jankowski, Maciej Wyczesany and Szymon Chorazy *

Multifunctional materials, which exhibit diverse physical properties, are candidates for the new generation of smart devices that realize many tasks simultaneously. Particular attention is given to single-phase multifunctional materials that offer the new physical effects induced by the coupling between introduced properties. Complexes of lanthanide(3+) ions are an attractive source of multifunctionality since they combine luminescent functionalities related to their f–f or d–f electronic transitions with magnetic anisotropy that originates from spin–orbit coupling and crystal-field effects. The resulting luminescent single-molecule magnets (SMMs) link the area of functional luminophores, applicable in light-emitting diodes or sensing, with the field of molecular magnets, applicable for high-density data storage, and offer additional advantages, *e.g.*, fruitful magneto-optical correlations and the switching of emission by a magnetic field. It was recently shown that luminescent lanthanide SMMs can provide multifunctionality that is richly expanded towards their sensitivity to solvent exchange, temperature, or light, as well as the generation of electrical properties, such as super-ionic conductivity and ferroelectricity, or non-centrosymmetricity- and chirality-related effects, *e.g.*, second-harmonic generation and circularly polarized luminescence. Here, we discuss the pioneering reports on multifunctional materials that use luminescent lanthanide SMMs, with the emphasis of our contribution relying on the functionalization of 4f metal complexes through their insertion into heterometallic d–f coordination compounds.

Received 24th January 2023,
Accepted 20th March 2023

DOI: 10.1039/d3cc00342f

rsc.li/chemcomm

Faculty of Chemistry, Jagiellonian University, Gronostajowa 2, 30-387 Krakow, Poland. E-mail: simon.chorazy@uj.edu.pl

Robert Jankowski

Robert Jankowski received his PhD degree in chemistry in 2021, completing his PhD studies at the Jagiellonian University, under the supervision of Prof. Barbara Sieklucka. He carried out research work concerning the synthesis and characterization of novel inorganic–organic materials based on octacyanidometallates combined with selected d- and f-metal complexes that can serve as multifunctional molecular magnets. Currently, he works as an assistant professor in the research group of Dr habil. S. Chorazy. His research area concerns the search for new materials based on metal complexes that work as multifunctional luminophores, linking magnetic and electrical properties with optical thermometry and chirality.

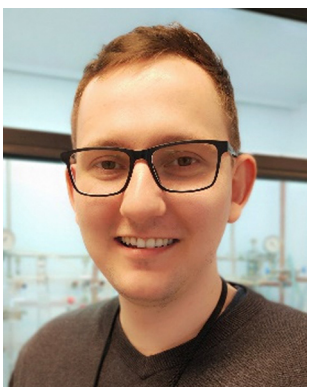

Maciej Wyczesany

Maciej Wyczesany started his research work at the Faculty of Chemistry, Jagiellonian University in 2016, working under the supervision of Prof. Barbara Sieklucka on magneto-luminescent molecular materials based on transition metal cyanido complexes. After he received his MSc degree in chemistry in 2019, he continued his scientific career in the PhD programme at the Jagiellonian University, realizing also the Diamond Grant project for young Polish scientists. Currently, he works in close collaboration with Dr habil. Szymon Chorazy, focusing on novel lanthanide-based materials incorporating tetracyanidometallates that exhibit diverse luminescent and magnetic functionalities which are sensitive to physical and chemical stimuli.

1. Introduction

Aiming at extreme miniaturization and efficiency, as well as the economical production of a new generations of smart optical, electronic, and magnetic devices, chemists and materials scientists have been encouraged to search for novel multifunctional materials that exhibit a few different physical properties.[1–4] Among the desired physical functionalities, one can count, for example, super-ionic conductivity, ferroelectricity, non-linear optical (NLO) effects, luminescence, ferromagnetism and electrochemical activity, and the responsivity of these effects to physical and chemical stimuli.[5–10] The combination of at least two of the above-listed properties in a multifunctional material can be realized in composite systems that are built of functional units, *e.g.*, magnetic nanoparticles covered by luminescent shells.[11–13] An alternative is offered by single-phase multifunctional materials whose various physical properties are designed at the molecular level within the homogenous matter.[14–16] They have been found to be attractive not only as the source of multitasking, which is the presence of a few different properties induced under the same conditions, but also in the generation of significant interactions between introduced effects.[17–19] If such coupling is strong, even novel physical cross-effects arise as shown in the unique examples of electro-optical, magneto-optical, or magneto-electric systems.[20–23] Multifunctional single-phase materials can be constructed by taking advantage of commonly applied solids, such as metal oxides or other inorganic matrices,[24,25] but the rational design of many functionalities for a single system is more accessible for molecular materials that are built of metal complexes and/or organic molecules.[26–28] The generation of targeted physical functionalities in molecule-based materials can be realized using the molecular building block approach where molecular components (metal ions, organic/inorganic molecules, ligands, or radicals) of the specific intrinsic properties are combined *via* covalent or coordination bonds as well as supramolecular interactions.[29–31] They are usually synthesized under soft laboratory conditions leading to the crystalline form, enabling their structural characterization. Owing to these advantages, molecule-based materials, which range from discrete molecules and supramolecular systems to coordination polymers (CPs) and metal–organic frameworks (MOFs), have been used widely as a source of multifunctionality, providing the unique groups of luminescent ferroelectric materials,[32,33] NLO-active magnets,[34,35] multiferroics,[36,37] and photoswitchable porous, ion-conductive or magnetic systems,[38–41] among others.[42–46]

Complexes of lanthanide (Ln) ions, especially trivalent ions, have been shown to be one of the most effective molecular building blocks for the construction of multifunctional molecule-based materials.[47–49] The primary interest in Ln(III)-based coordination assemblies has been devoted to their luminescent properties that are related to emissive f–f or d–f electronic transitions.[50–52] The photo- and electroluminescence of materials based on Ln complexes is adjustable through selection of the metal ion as well as the attached ligands which play a crucial role in achieving the high emission intensity through the ligand-to-metal energy-transfer process.[53–55] As a result, these materials have been found to be emissive in various parts of the UV-vis-NIR spectrum, exhibiting diverse optical features such as tunable multi-coloured luminescence, white-light emission, sensitized NIR emission, and up-conversion luminescence (UCL) that offers the conversion of NIR excitation to visible light.[56–60] These findings have provided a broad application horizon for luminescent materials based on Ln(III) complexes. It includes light-emitting diodes (LEDs), displays, optical data storage, anti-counterfeiting, bioimaging, and sensors.[61–68] Some Ln(3+) ions embedded in the proper coordination environment have also revealed strong magnetic anisotropy that originates from the combined contributions of the dominant spin–orbit coupling (SOC) and the smaller yet crucial crystal field effect.[69–71] As a result, selected Ln(III) complexes, especially those of Dy^{III}, Tb^{III}, or Er^{III}, exhibit slow relaxation of magnetization, which provides a magnetic hysteresis loop of molecular origin.[72–78] Such single-molecule magnets (SMMs) are expected to be a breakthrough in the pursuit of novel high-density data storage devices,[73,79] revealing also further application perspectives in molecular spintronics.[80]

The selection of an appropriate Ln ion and the design of its coordination environment can ensure the combination of luminescence and magnetic anisotropy. This makes Ln(III) complexes the best prerequisites for bifunctional emissive molecular nanomagnets[81–83] that are rarely achievable using other metal centres.[84] Luminescent SMMs have been constructed using a few different Ln ions, including visible-light-emissive Sm^{III}, Dy^{III}, and Tb^{III},[85–87] or NIR-emissive Nd^{III}, Er^{III}, and Yb^{III},[88–90] and have been investigated deeply towards magneto-optical correlations as well as the switching of emission using a magnetic field.[91,92]

The main synthetic strategy for luminescent molecular nanomagnets based on Ln complexes relies on the selection or design of organic ligands that ensure both the magnetic anisotropy as well as the efficient luminescence of the selected metal ion. This is a challenging task as single-ion anisotropy is

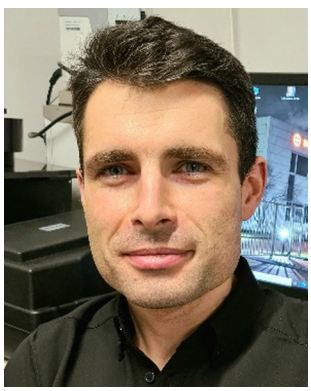

Szymon Chorazy

Szymon Chorazy has held a PhD degree in chemistry since 2014, finishing the international PhD-studies programme at the Jagiellonian University, under the supervision of Prof. Barbara Sieklucka in collaboration with Prof. Shin-ichi Ohkoshi (The University of Tokyo). He worked as an assistant professor in the group of Prof. S. Ohkoshi. Now, he is an associate professor at the Jagiellonian University where he received habilitation in 2019 and leads the Multifunctional Luminescent Materials Group. His research interests concern luminescent molecule-based materials based on metal complexes, including emissive magnets and porous materials, optical thermometers, as well as chiral luminophores, and phase transition systems.

generated by inducing the axial or planar arrangement of negatively charged donor atoms around the Ln ion, depending on the shape of its electron density,[93] whereas the sensitization of Ln(III) emission by attached ligands is connected with the energy of their donor excited electronic states.[94] Thus, both conditions have to be fulfilled, which can be achieved using purposefully designed ligands, usually based on expanded aromatic components, with the support of counter-ions and solvents.[84–87,89–92,95–99] To achieve multifunctional Ln-based molecular materials, including emissive SMMs, a particularly useful approach is based on the use of macrocycle ligands.[95–99] We and other groups have developed an alternative strategy that consists of using complexes of the second metal ion as metalloligands attached to the Ln ions.[88,100–102] Such a heterometallic synthetic approach to luminescent Ln(III)-based SMMs usually employs cyanido transition metal complexes as the metalloligands.[101,102] This idea was inspired by research on heterometallic d–d or d–f coordination assemblies built using polycyanidometallates, which are attractive molecular platforms for multifunctional materials that link magnetic phenomena, *e.g.*, spin transitions, magnetic ordering, or single-molecule magnetism, with other physical properties.[103–109] Both luminescent materials built from Ln(III) complexes and 4f-metal-based SMMs have been independently explored as the source of multifunctionality. The Ln(III) complexes were found to combine luminescent effects with second harmonic generation (SHG),[110–112] proton or electronic conductivity,[113,114] and catalytic activity,[115,116] as well as sensitivity to solvent molecules,[117–119] various chemicals,[120–122] and light.[123–125] Non-emissive Ln(III) molecular nanomagnets have also been successfully functionalized, in particular, towards chemical and photo-switching abilities,[126–129] ferroelectricity,[130] and chirality. The latter provides a pathway for NLO and other related optical and magneto-optical properties.[131–134] Taking advantage of efficient strategies for the construction of Ln-based luminescent SMMs and the perspectives for their further functionalization, as realized separately in the areas of Ln luminophores and Ln molecular magnets, our group and others have developed the novel scientific direction that is the design of multifunctional systems using Ln emissive SMMs as the molecular precursors. This approach is expected not only to enrich the multifunctionality by adding co-existing physical properties but also to induce interactions between the added functionalities and the magneto-luminescent character of the Ln(III) complexes.

In this review, we discuss the main findings in the emerging research trends concerning the multifunctionality of luminescent molecular nanomagnets based on Ln complexes. First, we present the illustrative concepts and advances regarding the luminescence and single-molecule magnetism of Ln(III)-based molecular materials. Then, we discuss the unique examples of stimuli-responsive luminescent Ln molecular nanomagnets, including those that are sensitive to chemicals, temperature, and light. In the next chapter, we highlight the pioneering reports on the generation of electrical effects, *e.g.*, proton conductivity and ferroelectricity, in the coordination compounds composed of emissive Ln(III)-based SMMs. Next, we discuss the results regarding the design of non-centrosymmetric and chiral structures based on luminescent Ln(III)-based SMMs that lead to such effects as SHG and circularly polarized luminescence (CPL). To conclude, we summarize the advances in the field, underlying the promising directions to be examined in the future. Throughout the review, we emphasize our contribution to the research area, which is related to the heterometallic synthetic approach that relies on the functionalization of Ln(III) complexes *via* their insertion into d–f cyanido-bridged systems.

2. Luminescence and single-molecule magnetism of lanthanide-based molecular materials

In the pursuit of multifunctional materials based on luminescent Ln-based molecular nanomagnets, primary attention should be given to the generation of luminescent functionalities co-existing with significant magnetic anisotropy. Below, we discuss briefly the respective fields regarding the luminescence and single-molecule magnetism of Ln complexes, their conjunction in magneto-luminescent systems, and, finally, a heterometallic synthetic approach towards such bifunctional materials that incorporate Ln complexes.

2.1 Luminescent functionalities in lanthanide(III)-containing molecular materials

The Ln series (Fig. 1) comprises elements which, in their metallic form, have the electronic configuration of $[Xe]6s^24f^x$, where x is the number of the Ln in the series from $x = 1$ for La to $x = 14$ for Yb and Lu (the latter has an extra electron on the 4d orbital). The exceptions are La, Ce, and Gd, in which one of the 4f electrons is promoted to the 5d orbital. All Ln metals are prone to oxidation to the most common third oxidation state in which their electronic configuration is $[Xe]4f^{x-1}$ (La^{3+} to Yb^{3+}) or $[Xe]4f^{14}$ (Lu^{3+}).[94] Due to the tendency to empty, half-fill, or fill their 4f shell, some of the Ln ions can adopt a second or fourth oxidation state, *e.g.*, Eu^{2+} ($4f^7$) or Ce^{4+} ($4f^0$).[135,136] These less common Ln ions have been explored as the source of emission;[137] however, here we will focus on the trivalent Ln ions as they have been used for the construction of luminescent SMMs.

The emission of Ln(3+) ions ranges from the UV (*e.g.*, Gd^{3+}) through the visible (*e.g.*, Ce^{3+}, Sm^{3+}, Eu^{3+}, Tb^{3+}, and Dy^{3+}), to the NIR (*e.g.*, Nd^{3+}, Er^{3+}, and Yb^{3+}) parts of the electromagnetic spectrum, making them attractive in numerous applications.[83,94] It is important to note that the Ln(3+) emission stems from 4f–4f electronic transitions with the exception of Ce^{3+}, for which 5d–4f electronic transitions are responsible for visible-light emission.[52] Therefore, most of the electronic transitions that govern their emission are carried out within the 4f sub-shell, which is effectively shielded by the 5s and 5p sub-shells, lowering the impact of the environment on the emission. This intrinsic protection of 4f orbitals from the external conditions impacts their emission patterns, as the related bands are narrow and their energy positions tend almost not to vary between systems; thus, they are easily assignable to the respective Ln ion (Fig. 1). Another consequence of the 4f–4f nature of Ln(3+) emission is their intrinsic low probability

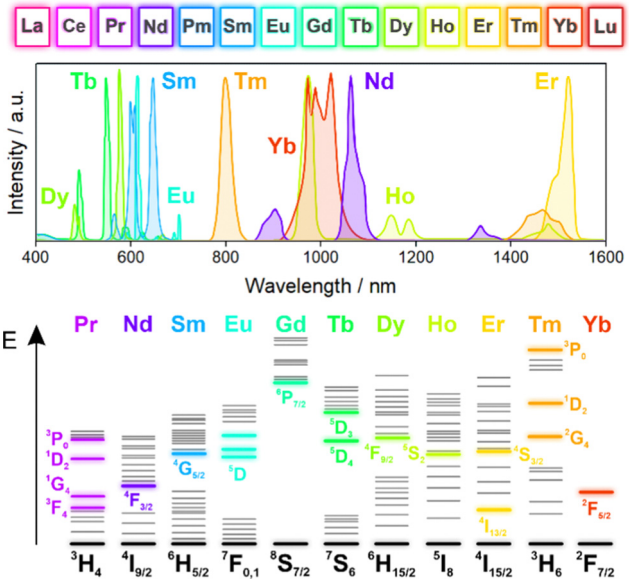

Fig. 1 Ln series of elements (top) together with the typical photoluminescence spectra of their trivalent ions in the vis-to-NIR range (middle) and the corresponding energy level diagrams (bottom, where the main emissive states are marked by colour). Note that the colours used in the spectra do not resemble the actual emission colours of the respective Ln ions.[94]

associated with their parity-forbidden character. As a result, the photon absorption cross-section, as well as the intensity of the emissions and the quantum yield tend to be small. However, due to thermal vibrations, which lead to the temporary breaking of symmetry, such transitions become possible.[53]

A large number of strategies have been developed to enhance the parameters of the Ln(3+)-based emission. Notably, the insertion of Ln(3+) ions into a non-centrosymmetric coordination environment enables the 4f orbitals to be partially admixed with orbitals of opposite parity, hence allowing the transitions.[138] Another, and the most exploited, approach involves the use of a sensitizing molecular building block, commonly referred to as an antenna,[94] that is capable of absorbing the energy of photons and transferring the energy to the Ln(3+) ion, bypassing the excitation route that involves forbidden transitions. Both organic and inorganic moieties can be employed for sensitization of the Ln(3+) emission if two main requirements are fulfilled.[139–142] Firstly, an antenna should efficiently harvest the energy through exciting-photon absorption, and secondly, the antenna must be able to transfer the energy to the Ln(3+) ion. A great number of organic ligands with a system of conjugated bonds or aromatic rings are usually efficient photon energy harvesters, although they are not guaranteed to be able to funnel this energy to the Ln(3+) ions. As the organic molecule absorbs the energy, and its singlet excited state (S_n) becomes occupied, the electron usually quickly relaxes to the ligand's lowest triplet state (T_1), which becomes the donor state in ligand-to-metal energy transfer. The efficiency of this process is dependent on the relative position of the T_1 level within the ligand and the emitting level of the Ln(3+) ion. To maximize the emission quantum yield, the T_1 energy level of the ligand should be located above the Ln emitting level with an energy difference that is small enough for energy transfer yet large enough for thermally activated energy back-transfer to be inactive. Many research groups have undertaken the challenge to design highly-emissive Ln(III)-based molecular materials, employing the above-mentioned strategy to take advantage of the variety of accessible Ln(III)-based optical functionalities.[47,143–148]

One of the functionalities explored for the luminophores built using Ln(III) complexes is white-light emission (WLE), which is applicable in LEDs and displays.[57,149] It can be realized through the insertion of close-to-white-light-emitting molecular components, such as some Ln(3+) ions, into the material with the capability of tuning the emission, *e.g.*, by modifying the crystal field. This approach can be exemplified by the work of Pecoraro *et al.* on Ga^{3+}/Dy^{3+}-metallacrowns that show Dy^{3+}-centred emission.[150] Their WLE is tuned through modification of the coordination environment within the polynuclear moiety, including the $[DyGa_4(shi)_4(bz)_4]^-$ (shi = salicylhydroxamate, bz = benzoate) molecular anion and its relatives (1–5, Fig. 2a and b).[150] The authors used the tunable emission that originates solely from Dy(III) $^4F_{9/2} \rightarrow {}^6H_J$ transitions. Alternatively, WLE is realized by mixing multiple Ln ions, *e.g.*, Ce^{3+}, Eu^{3+}, and Tb^{3+},[151] often accompanied by organic luminophores,[152] with complementary emission colours.[57,149] The multi-Ln strategy is also appealing in the search for materials with tunable multi-coloured emission. In particular, the Eu^{3+} and Tb^{3+} pair has aroused great interest due to their respective red and green emissions.[149,153] For instance, some of us reported a series of coordination chains $\{[Eu^{III}_x Tb^{III}_{1-x}(3\text{-OHpy})_2(H_2O)_4][Co^{III}(CN)_6]\}\cdot H_2O$ (3-OHpy = 3-hydroxypyridine, x from 0 to 1).[154] Depending on the Eu^{3+} and Tb^{3+} composition and the excitation, these materials reveal luminescence ranging from green, through yellow and orange, to red. In this system, not only the 3-OHpy ligand but also the $[Co^{III}(CN)_6]^{3-}$ ion play a modulating role for the Ln(III) emission. The combination of Eu(III) and Tb(III) complexes in a single-phase material has also been used in the construction of luminescent thermometers, which are systems that are capable of changing their emission, such as the colour, intensity ratio, or lifetime, in response to temperature variation.[68,141,155] Such thermometers typically exploit the intensity ratio between the emission peaks assignable to Eu^{III} and Tb^{III} centres, related to their f–f electronic transitions, $^5D_0 \rightarrow {}^7F_{0,1,2,3,4}$ (Eu^{3+}) and $^5D_4 \rightarrow {}^7F_{2,3,4,5,6}$ (Tb^{3+}). Taking advantage of the proximity of their emitting levels, it is possible to design a molecular antenna that is able to transfer the energy to both Ln ions. Appropriate tuning of the sensitizers' donor energy level combined with the thermal dependence of the energy transfers leads to thermally-induced variation in the Ln(III) emission bands. This can lead to the ratiometric quantification of the thermal response of systems using the ratios between the intensities of the Eu^{3+}- and Tb^{3+}-centred emission bands. This approach can be exemplified by Hasegawa *et al.*, who obtained $[EuTb(tmh)_6(dpbp)]$ molecules supported by six tetramethylheptanedionate (tmh) ligands and a phosphine oxide linker (dpbp, Fig. 2c and d).[156] Due to the role of a ligand-to-metal charge-transfer state on the Eu(III) site, the emission colour changes from red to green with increasing temperature, which is unusual as the related optical

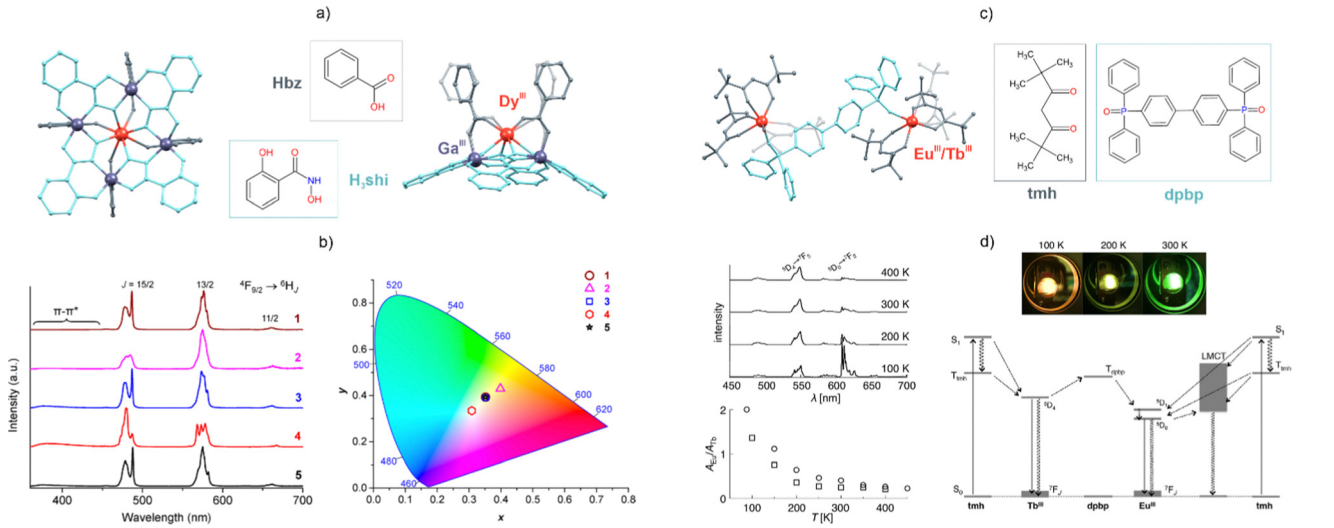

Fig. 2 (a) Structural view of the $[Dy^{III}Ga^{III}_4(shi)_4(bz)_4]^-$ (shi = salicylhydroxamate, bz = benzoate) molecular anion[150] and (b) emission spectra under 340 nm excitation for the series of its derivatives (1–5) shown alongside the CIE 1931 chromaticity diagram that depicts the respective emission colours. (c) Structural view of the $[EuTb(tmh)_6(dpbp)]$ (tmh = tetramethylheptanedionate, dpbp = 4,4′-bis(diphenylphosphoryl)biphenyl) dinuclear complexes[156] and (d) their temperature-dependent emission spectra gathered in the 100–400 K range, presented with the ratio of the spectral areas of Eu^{3+}- and Tb^{3+}-centred emission bands, photos of the respective emission colours at 100, 200, and 300 K, and the related energy diagram showing the nature of the electronic transitions and energy transfer processes in the system. Part (b) was adapted with permission from ref. 150. Copyright 2020 American Chemical Society. Part (d) was adapted with permission from ref. 156. Copyright 2018 John Wiley & Sons.

response of most of MOFs with Eu^{3+} and Tb^{3+} ions is the opposite.[141,155] Other pairs of Ln ions, such as Tb^{3+}/Dy^{3+} or Nd^{3+}/Yb^{3+}, have also been explored for optical thermometry.[157,158]

Among other optical effects exploited for Ln(III) complexes, it is worth mentioning UCL, in which the chromophore absorbs two or more photons leading to the emission of a shorter wavelength.[159] This non-linear optical process occurs through a few different mechanisms, *e.g.*, the cooperative sensitization from two Yb(III) centres to the single Er(III) centre. As a result, the relatively-low-energy NIR excitation, *e.g.*, the 980 nm laser source, that is suitable for the Yb(III) excitation can be employed to generate visible-light emission, which opens great application horizons, especially in bioimaging or theranostics.[160] Primarily, UCL effects have been recognized in mixed-Ln fluoride solids;[161] however, molecular materials incorporating heterometallic coordination complexes based on Ln(3+) ions, *e.g.*, Er^{3+}, Yb^{3+}, or Tb^{3+}, have recently been obtained.[60,162,163]

As discussed above, most of the Ln(3+)-centred emissive electronic transitions are of the Laporte-forbidden 4f–4f nature. However, Ce(III) complexes feature symmetry-allowed 5d–4f emissive electronic transitions. They are much more sensitive to changes in the coordination environment than 4f–4f electronic transitions,[164] and have been utilized in efficient emission tuning using external stimuli for optical sensing applications, *e.g.*, in pressure sensors.[52,165,166]

2.2 Lanthanide single-molecule magnets

SMMs are built of metal complexes that exhibit significant magnetic anisotropy, which can lead to the slow relaxation of magnetization, resulting in the appearance of magnetic hysteresis of molecular origin below the so-called blocking temperature (T_B).[167–169] The complexes of Ln ions, in either 3+ or 2+ oxidation states,[168,170–172] are great candidates for the construction of SMMs as they can exhibit large magnetic anisotropy that corresponds to the combined roles of a large SOC and a smaller yet critical crystal field (CF) effect.[82,83,173,174] The first phenomenon, SOC, is typically significant for the ions of heavy metals, such as Ln metals. Moreover, the partially occupied 4f orbitals of Ln ions are effectively shielded from the coordination environment by the filled $5s^2$ and $5p^6$ orbitals, ensuring an almost exclusive electrostatic character of interaction between ligands' donor atoms and the Ln^{3+} ion itself. As a result, the CF effect is much weaker than the SOC; however, this influence of the attached ligands is crucial for the SMMs as it is responsible for the energy splitting of the large unquenched angular momentum states of the ground multiplet governing the magnetism. It results in the key bistability between the two m_J levels accompanied by the energy barrier for the reversal of a magnetic moment.[69,82,83,173,174] The general approach to the rational design of SMMs based on Ln complexes (Ln-SMMs) is to adjust the CF effect by playing with the symmetry of the complex and the alignment of the ligands. The intuitive rules for such a design were provided by Rinehart and Long.[93] Their model takes into consideration the electron density of the Ln ion and selected ligands. For maximization of the magnetic anisotropy, by ensuring the largest m_J value for the 4f metal ions of the equatorially expanded oblate 4f electron distribution, *e.g.*, Tb^{3+}, Dy^{3+}, or Ho^{3+},[168,175,176] it is preferred to generate the ligand electron density above and below the Ln ion. Such an alignment can be realized by placing the ligands with the largest electron density at the axial positions (Fig. 3). By contrast, the Ln ions of the axially expanded prolate 4f electron distribution, *e.g.*, Er^{3+} or Yb^{3+},[78,177] require the ligands with largest electron densities to occupy equatorial positions.

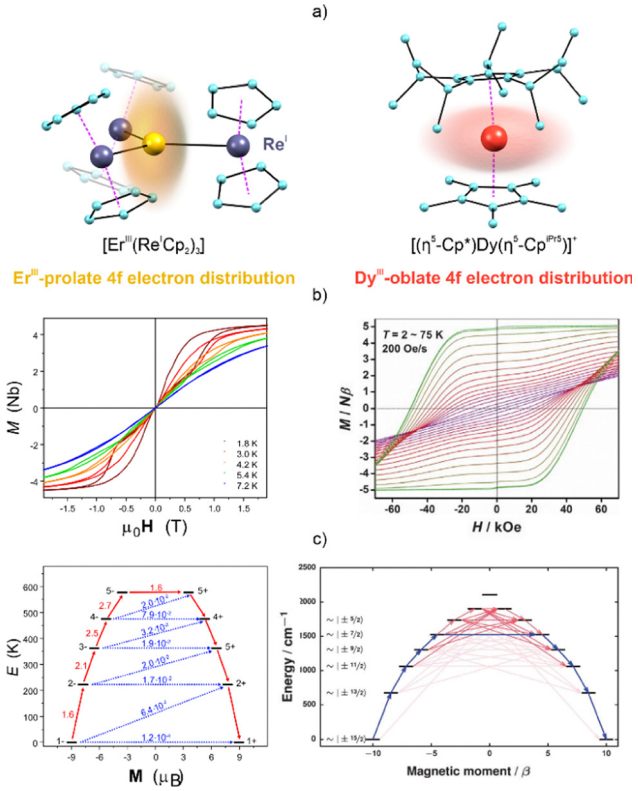

Fig. 3 (a) Graphical representation of prolate (left) and oblate (right) 4f-shell electron distribution *via* examples of $[Er^{III}(Re^{I}Cp_2)_3]$ and $[(\eta^5\text{-Cp}^*)Dy^{III}(\eta^5\text{-Cp}^{iPr5})]^+$ molecules,[73,187] (b) their magnetic hysteresis loops at the indicated temperatures (left for Er^{III}, right for Dy^{III}), and (c) the *ab initio*-calculated energy splitting of the ground multiplet with the most probable relaxation pathways visualized (red coloured arrows for Er^{III} on the left, dark blue coloured arrows for Dy^{III} on the right). Parts (b, left) and (c, left) were adapted under terms of the CC-BY license, ref. 187. Copyright 2022, published by Springer Nature. Parts (b, right) and (c, right) were adapted with permission from AAAS, from ref. 73.

Following these guidelines, a considerable number of Ln-SMMs have been obtained, mainly using Tb^{III}, Dy^{III}, Ho^{III}, and Er^{III} complexes with the highest accessible m_J levels.[168,175,176,178]

The best SMMs are usually achieved using Ln ions with an oblate 4f electron distribution, Dy(3+) ions in particular as they have a half-integer angular momentum, and thus the magnetic bistability is ensured by their Kramers nature.[69,178] This is opposite to non-Kramers-type Tb(3+) and Ho(3+) ions, which demand a high-symmetry complex or the support of other effects, *e.g.*, a hyperfine interaction, for achieving the SMM features.[168,176] In particular, Dy^{III}-containing metallocene complexes are in the lead in terms of the size of the energy barrier for spin reversal. This is exemplified by the ground-breaking sandwiched dysprosocenium molecule $[(Cp^{ttt})_2Dy^{III}][B(C_6F_5)_4]$ (Cp^{ttt} = 1,2,4-tri(*tert*-butyl) cyclopentadienide).[179] This system exhibits an anisotropic energy barrier of 1233 cm^{-1} and magnetic hysteresis below 60 K. The liquid nitrogen temperature limit was broken by Layfield and co-workers.[73] They synthesized a new dysprosocenium system, $[(Cp^*)Dy^{III}(Cp^{iPr5})][B(C_6F_5)_4]$ (Cp^* = pentamethylcyclopentadienyl; Cp^{iPr5} = pentaisopropylcyclopentadienyl), with a more axial alignment of the Cp-type ligands, ensuring an energy barrier of 1541 cm^{-1} and a T_B value of 80 K (Fig. 3).

SMMs have mainly been studied in the crystalline form containing the spins embedded in the crystal lattice. The mutual spin-lattice interactions involving phonons are the origin of multiple magnetic relaxation pathways. The three most common spin-lattice relaxation mechanisms operating in SMMs include (i) the direct process involving relaxation from $-m_J$ to $+m_J$ with the emission of a single lattice phonon, (ii) the two-phonon-assisted Orbach process through the anisotropic energy barrier, and (iii) the Raman relaxation involving a two-phonon process occurring through a virtual excited state.[69,180] Process (i) occurs only in an applied magnetic field, while (ii) and (iii) can co-exist under a zero-direct current (zero-dc) field. The Orbach process is tuned through the coordination environment of the 4f metal ion as it corresponds directly to the CF effect. A difficult issue is to control the Raman relaxation, which is related to the presence of lattice vibrations that can disturb the SMM properties, even for a large magnetic anisotropy.[181–183] In addition, if the magnetic Ln(II/III) system shows non-negligible transverse anisotropy, quantum tunneling of the magnetization (QTM) is observed. The occurrence of QTM in the majority of Ln-based SMM systems implies the presence of a swift relaxation pathway and drastically limits the relaxation times. One of the strategies to overcome this effect is the use of specific symmetry elements to reduce transverse magnetic anisotropy. Tong *et al.* reported exhaustive studies concerning the role of symmetry in slow magnetic relaxation.[184] It was shown that the S_8/D_{4d}, C_{5h}/D_{5h}, C_{6h}/D_{6h}, or S_{12}/D_{6d} symmetry groups can ensure the minimal transverse CF, thus quenching the QTM. Even though none of these ideal geometries can be easily reached in the crystalline material, achieving a symmetry close to the aforementioned ones should improve the SMM efficiency. This can be exemplified by the pentagonal bipyramidal complexes of $[Dy(cy_3PO)_2(H_2O)_5]Cl_3\cdot(cy_3PO)\cdot H_2O\cdot EtOH$ and $[Dy(cy_3PO)_2(H_2O)_5]Br_3\cdot 2(cy_3PO)\cdot 2H_2O\cdot 2EtOH$ (cy_3PO = tricyclohexylphosphine oxide).[185] These complexes exhibit energy barriers of ~500 K and magnetic hysteresis up to 20 K, as a result of the closely ideal D_{5h} local symmetry and the axially aligned oxide ligands. Due to a prolate nature of the 4f electron distribution, distinguishable strategies have been employed to achieve Er(III)- and Yb(III)-based SMMs.[69,184,186] In particular, the Er(III) SMMs were found to be promising, as exemplified by their trigonal planar or pyramidal complexes bearing negatively charged ligands at equatorial positions.[78] Recently, transition metal ions were employed as ligands for Er(III)-based SMMs.[187] The trigonal planar $[Er^{III}(Re^{I}Cp_2)_3]$ complex exhibits a unique structure in which the Er^{3+} ion is surrounded solely by diamagnetic Re^{I} centres (Fig. 3). The transition metal centres, which act as donor atoms, provide a large magnetic anisotropy, giving magnetic hysteresis up to 7.2 K.

Another strategy that is worth mentioning towards high-performance molecular nanomagnets involves providing an efficient Ln–Ln exchange interaction, which is challenging due to the 4f electrons being shielded.[188,189] However, the recent work of Long *et al.* showed that this approach might be fruitful, as was presented for the mixed-valence $[(Cp^{iPr5})_2Dy_2I_3]$ complex.[190]

In this material, valence delocalization ensures the strong parallel alignment of σ-bonding and f electrons within both Ln centres, generating a high-spin ground state and large magnetic anisotropy, which gives a huge coercive magnetic field that shows a lower bound of ~14 T below 60 K.

2.3 Linking luminescence with single-molecule magnetism in lanthanide-based molecular materials

The use of intrinsically emissive Ln(III) centres in the construction of molecular nanomagnets has indicated the emergence of bifunctional luminescent SMMs.[82,191] This research pathway is a natural course after the growth of a multitude of Ln^{III}-SMM systems over the past decades, which drew the attention of scientists to investigate the eventual interplay of their designable luminescent and magnetic properties. This attractive possibility was first noticed by Hendrickson *et al.* for the non-Ln system. They prepared $\{Mn^{II}_2Mn^{III}_2\}$ coordination clusters that demonstrated SMM properties together with ligand-based fluorescence.[84]

Later, Ln(3+) ions appeared at the forefront of research into luminescent SMMs due to their emissive f–f or d–f electronic transitions (see Section 2.1) as well as their significant magnetic anisotropy related to their large spin–orbit coupling and crucial crystal field effect (see Section 2.2). However, the optimization of both luminescence and SMM features is a difficult task.[82,191] In particular, when considering the choice of a suitable Ln(3+) ion, one should keep in mind the oblate/prolate nature of its 4f electron distribution that governs the anisotropy character (Fig. 3) as well as the magnitude of its magnetic moment. It is also essential that the most intense photoluminescence is observed for Ln(III) centres that possess emissive states well separated from each other, which limits the non-radiative relaxation (Fig. 1). Taking these prerequisites into account, the most common selection for luminescent SMMs is directed towards yellow-to-white-emissive Dy(III) and NIR-emissive Yb(III) centres,[86,90] as well as, to a lesser extent, green-emissive Tb(III) or NIR-emissive Er(III) or Nd(III) centres.[87–89] A critical role can be played by supporting ligands that provide three important functions: (i) efficient ligand-to-metal energy transfer to the Ln^{3+} ion, enhancing its emission; (ii) effective adjustment of the coordination sphere, ensuring a protective shell to minimize emission deactivation processes; and (iii) enabling slow relaxation of the magnetization to be observed by placing the negative charge at appropriate positions and limiting the often disturbing inter-Ln magnetic interactions.[82,83,191]

One of the pioneering examples of the successful combination of both functionalities in a Ln^{III}-based system was presented in 2009 by Gao and collaborators in work concerning the Dy^{III} complex bearing calixarene ligands.[192] From that point onwards, the family of Ln(III)-based luminescent SMMs grew rapidly, as discussed in dedicated review articles.[82,83,191] However, both functionalities were usually investigated independently without attempting to study their possible magneto-optical correlation. The first attempts to correlate these two properties and scrutinize the details of slow relaxation dynamics based on emission spectra were made in 2012.[81] The emission spectrum was proved to contain information on the energy gap between the ground and the excited m_J state. By comparing this value with the anisotropic energy barrier, determined from alternating-current (ac) magnetic measurements, one can gain the relevant arguments for discussion of the mechanisms of the slow relaxation of magnetization. Sessoli *et al.*[81] used this methodology in the magneto-optical characterization of the $[Dy^{III}(dota)(H_2O)]^-$ (dota = 1,4,7,10-tetraazacyclododecane-1,4,7,10-*N*,*N*′,*N*″,*N*‴-tetraacetate) complex. Through analysis of its room-temperature emission spectrum, one can distinguish well-resolved emission bands related to the $^4F_{9/2} \rightarrow {}^6H_{15/2,13/2,11/2}$ electronic transitions. The energy gap between the ground and the first excited m_J energy levels within the highest-energy $^4F_{9/2} \rightarrow {}^6H_{15/2}$ emission band was determined as 53 cm^{-1}, which was postulated to correspond to the energy barrier of an Orbach relaxation. The energy barrier estimated based on the ac magnetic data turned out to be lower, at 42 cm^{-1}. The discrepancy was ascribed to the presence of other magnetic relaxation pathways, and thus the luminescence was concluded to be an indicator for the degree of occurrence of non-Orbach magnetic relaxation routes. Since this work, emissive Ln-SMMs have attracted substantial attention, due mainly to the magneto-optical correlations that take advantage of the emission spectra in the analysis of the Ln-SMM performance.[90,193–197] An elegant example was presented by Murugesu *et al.* who performed a thorough investigation of the magnetic and optical properties of the $[Yb^{III}_2(valdien)_2(NO_3)_2]$ complex (valdien = dianion of the N1,N3-bis(3-methoxysalicylidene)diethylenetriamine), which is a unique luminescent thermometer that exhibits SMM behaviour (Fig. 4).[198] Using the high-resolution low-temperature emission spectrum related to the Yb(III)-based NIR-luminescence, the authors provided a complete assignment of the energetic profile for the ground multiplet. This was further used in the discussion of magnetic relaxation which was found to be dominated by the Raman process. Moreover, this system exhibits one of the highest effective anisotropic energy barriers among the Yb^{III} SMMs.

Luminescent SMMs have turned out to be convenient candidates for magneto-optical systems in which the emission can be tuned *via* a magnetic field.[91,92,199] This effect was demonstrated by Gao *et al.* for the Dy(III)-based molecular nanomagnet bearing a naphthyridine-containing ligand.[92] The authors observed that the evident shifts and splitting of the analyzed emission bands correlated with the occurrence of the Zeeman effect under an applied pulsed magnetic field in the range of 0–36 T. It should be mentioned that scrutinizing the Zeeman splitting of the two lowest doublets of the Dy(III) ground term $^6H_{15/2}$ under selected values of the magnetic field led to the extraction of the average *g* factor. The influence of a magnetic field on the luminescence was detected in the $[Dy^{III}_2(bpm)(tfaa)_6]$ SMM (bpm = 2,2′-bipyrimidine, tfaa = 1,1,1-trifluoroacetylacetonate) (Fig. 5a).[199] In its very-low-temperature emission spectrum (Fig. 5b) one can observe the influence of a magnetic field on the luminescence that originates from the $^4F_{9/2} \rightarrow {}^6H_{13/2}$ transition. Strengthening of the applied field up to 14 T prompted a significant broadening of the emission spectrum profile as well as a clear splitting of the 0–0 line. The Zeeman

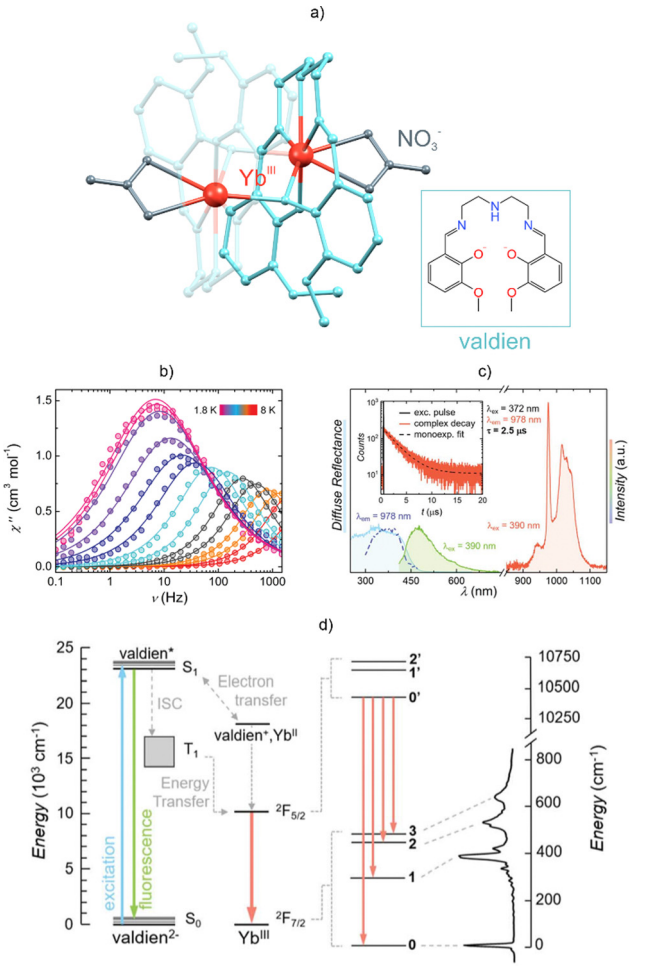

Fig. 4 (a) Crystal structure of the $[Yb^{III}_2(valdien)_2(NO_3)_2]$ molecule (valdien = dianion of N1,N3-bis(3-methoxysalicylidene)diethylenetriamine),[198] (b) magnetic and luminescent properties, including the frequency dependency of the out-of-phase magnetic susceptibility for the indicated temperatures at H_{dc} = 1 kOe, (c) spectroscopic characteristics of its solid-state absorption spectrum (cyan), emission spectrum in the visible (green) and NIR (orange) regions for 390 nm excitation, and the related excitation spectrum (blue dashed line), shown with the emission decay profile in the inset, and (d) schematic energy level diagram with the *ab initio*-calculated energy splitting of the ground multiplet compared with the high-resolution emission pattern gathered at 77 K. Parts (b–d) were reproduced from ref. 198 with permission from the Royal Society of Chemistry.

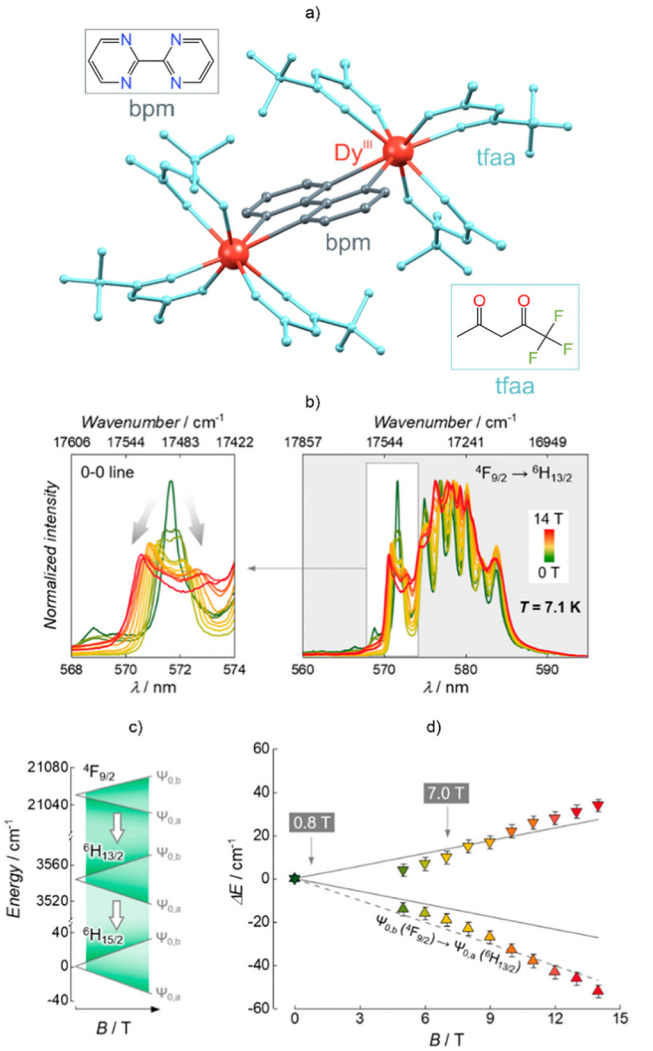

Fig. 5 (a) Crystal structure of the $[Dy^{III}_2(bpm)(tfaa)_6]$ molecule (bpm = 2,2′-bipyrimidine, tfaa = 1,1,1-trifluoroacetylacetonate),[199] (b) fragment of its low-temperature emission spectrum under the influence of a magnetic field, (c) related scheme of Zeeman splitting calculated for the three indicated Dy(III)-centred emissive transitions, and (d) comparison between the calculated (solid lines) and experimental (coloured triangles) Zeeman splitting of the $^6H_{13/2}$ level, shown together with the expected trend taking into account the Zeeman splitting of the emissive $^4F_{9/2}$ level (dashed line). Parts (b–d) were adapted from ref. 199, which was published under the ACS AuthorChoice license.

splitting was calculated for a set of low-lying levels: $^4F_{9/2}$, $^6H_{13/2}$, and $^6H_{15/2}$ (Fig. 5c). This found a good reflection in the experiment, as demonstrated for the Zeeman splitting of the $^6H_{13/2}$ level using the energy position of the related 0′–0 line (Fig. 5d). Moreover, this material exhibits luminescent thermometry related to the variable intensities of the selected emission regions. The temperature self-monitoring capability was altered using the magnetic field.

2.4 Heterometallic approach towards luminescent lanthanide-based molecular nanomagnets

Ln(III) complexes offer a plethora of luminescent and magnetic functionalities as well as their combinations (see above), which enable them to be used in various technological branches.[61–68,79,80] However, the formulation of strategies for the effective generation, enhancement, and modulation of the related opto-magnetic features of Ln(III) complexes remain a great challenge. This is typically achieved through the application of carefully selected or designed organic ligands that surround the Ln(3+) ion in the lattice. These supporting molecular components influence the Ln(III)-centred photoluminescence and/or magnetic behaviour through a variety of means, ranging from the crucial modification of the 4f metal ion coordination environment, which governs the efficiency of the antenna-to-metal energy transfer, to the direct induction of new functionalities, *e.g.*, by introducing chirality into the system that moderates the structure and optical properties.[82,83,191] Besides the organic

components, to a lesser extent, the inorganic ligands and the non-innocent counter-ions have also been explored for the analogous design of luminescent Ln-SMMs.[200–202]

Our group and others found a great alternative in the formation of emissive Ln-SMMs *via* the incorporation of 4f metal ions into heterometallic coordination systems. In particular, a considerable number of d-block metal ions with the support of organic and/or inorganic ligands were combined with Ln(III) centres into molecule-based materials that showed luminescent and/or magnetic properties.[108,187,203–207] Among them, besides or even instead of organic ligands, metalloligands, which are also usually based on d-block metal complexes, were successfully explored for control of the coordination sphere of Ln(3+) ions towards efficient emission and SMM features.[100–102,205–207]

In this context, a specific group of d–f coordination systems based on polycyanidometallates, depicted using the formulas $[M(CN)_x]^{n-}$ or $[M(CN)_x(L)]^{n-}$ (M = transition metal ions, L = supporting blocking ligands, *e.g.*, 2,2′-bipyridine), is a great source of luminescent, magnetic, and magneto-luminescent molecular materials.[105–109,208–210] They offer intermetallic cyanido bridges that ensure the strong binding of two different metal centres, which is suitable for efficient exchange magnetic coupling that is applicable for the design of molecule-based ferro(I)magnets[105,107,211] but which can be also used in providing efficient metal-to-metal energy transfer that enhances, for example, the Ln(III)-based emission.[208,210,212–215] Moreover, most cyanido complexes are strong absorbers of UV light, while the strong ligand field provided by the cyanido ligands can often shift the light absorption outside the visible-to-NIR ranges.[108,210,216,217] As a result, cyanido transition metal complexes appear to be good sensitizers of Ln luminescence.[208,210,212–215] We followed this approach and incorporated Eu(3+) and Tb(3+) ions into coordination polymers utilizing tetracyanidometallate ions of Pt(II) and Pd(II) as molecular bridges (Fig. 6a and b).[218] They form hybrid organic–inorganic coordination chains, $\{[Ln^{III}(H_2O)_4(terpyO_3)]_2[M^{II}(CN)_4]\}[M^{II}(CN)_4]_2{\cdot}8H_2O$ (Ln = Eu, Tb; M = Pt, Pd; $terpyO_3$ = 2,2′:6′,2″-terpyridine *N*,*N*′,*N*″-trioxide), that exhibit strong green-to-yellow-to-red Ln(III)-based photoluminescence which is strongly dependent on the temperature variation. The Eu(III)- and Tb(III)-centred emissions are effectively sensitized by the $terpyO_3$ ligands and $[M^{II}(CN)_4]^{2-}$ ions, while the emission colour is tuned by the Eu-to-Tb metal ratio. A pair of heterobi-Ln materials with the optimized metallic compositions of $\{Eu_{0.6}Tb_{1.4}Pt_3\}$ and $\{Eu_{0.6}Tb_{1.4}Pd_3\}$ was employed as optical molecular thermometers utilizing the intensity ratios of the Tb(III)- and Eu(III)-based emission bands or the ratios between the related emission lifetimes. Both systems were found to be effective ratiometric thermometers with the best performance represented by the relative thermal sensitivity (S_r) above the limit of 1% K^{-1} for the broad temperature range of 180–300 K, and the highest maximal S_r of 3.26% K^{-1} was reached for emission-lifetime-based thermometry at 239 K. The use of polycyanidometallate ions in the system enabled the efficient modulation of the thermometric characteristics by tuning the sensitivity and effective sensing range of the material. This was correlated with the d-block-metal-dependent energies of the vibrational modes of the cyanido ligands as well as other molecular components. We also employed the tetracyanido complexes of Pt(II) and Pd(II) together with dicyanidometallate ions of Au(I) and Ag(I) as the advanced sensitizers for red-emissive Eu(III) centres (Fig. 6c and d).[219] This was shown for the family of two-dimensional coordination networks, $\{[Eu^{III}(4,4'\text{-bpdo})(H_2O)_2][M^{II}(CN)_4]\}{\cdot}[M^{I}(CN)_2]{\cdot}H_2O$ (M^{II} = Pt^{II}, Pd^{II}; M^{I} = Au^{I}, Ag^{I}; 4,4′-bpdo = 4,4′-bipyridine *N*,*N*′-dioxide), which exhibit room-temperature Eu(III)-centred red emission that is sensitized through metal-to-metal-to-ligand charge-transfer (MMLCT) states related to the formation of d^8–d^{10} heterometallophilic interactions. Therefore, the $\{M^{II}M^{I}\}$ molecular entities that involve two types of cyanido complex play a crucial sensitizing role, whereas the further modulation of the energy transfer *via* the additional organic 4,4′-bpdo linkers was also noted.

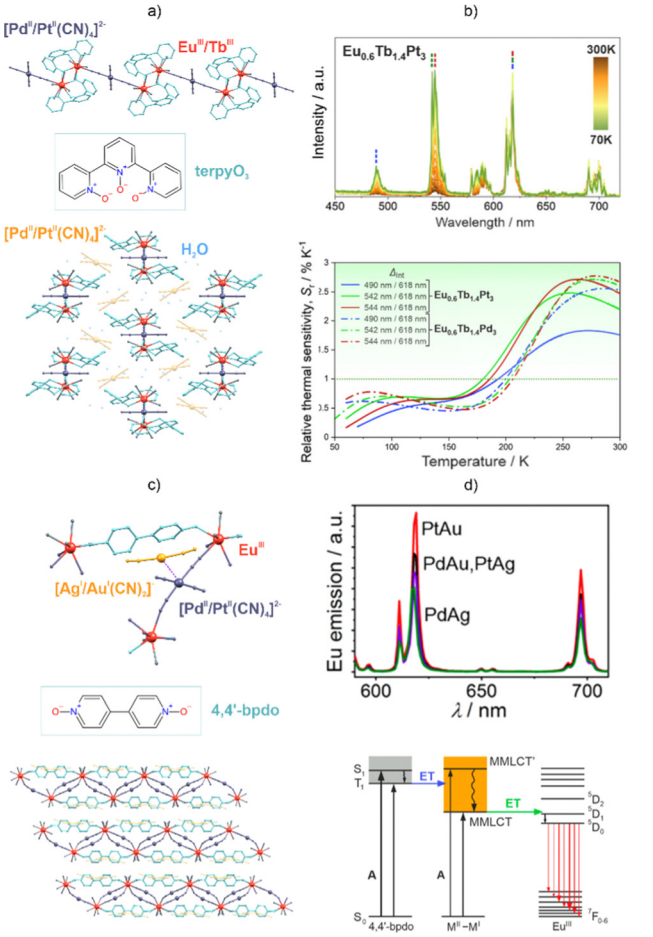

Fig. 6 (a) Structural view of the $\{[Ln^{III}(H_2O)_4(terpyO_3)]_2[M^{II}(CN)_4]\}[M^{II}(CN)_4]_2{\cdot}8H_2O$ (Ln = Eu, Tb; M = Pt, Pd; $terpyO_3$ = 2,2′:6′,2″-terpyridine *N*,*N*′,*N*″-trioxide) coordination chains,[218] (b) temperature-variable emission spectra for the $\{Eu_{0.6}Tb_{1.4}Pt_3\}$ analogue under 323 nm excitation (top), shown together with the temperature dependence of the relative thermal sensitivity for two representative compounds under the indicated excitation conditions (bottom). (c) Structural view of the $\{[Eu^{III}(4,4'\text{-bpdo})(H_2O)_2][M^{II}(CN)_4]\}{\cdot}[M^{I}(CN)_2]{\cdot}H_2O$ (M^{II} = Pt^{II}, Pd^{II}; M^{I} = Au^{I}, Ag^{I}; 4,4′-bpdo = 4,4′-bipyridine *N*,*N*′-dioxide) layered coordination networks,[219] (d) their emission spectra for various d^8–d^{10} metal combinations (top), and the schematic energy level diagram depicting the nature of the electronic transitions and energy-transfer processes (bottom). Part (b) was reproduced from ref. 218 with permission from the Royal Society of Chemistry. Part (d) was adapted with permission from ref. 219. Copyright 2020 American Chemical Society.

The sensitization of the Ln emission was found to depend on the combination of d-block metal ions, leading to the optimized luminescence for the heaviest {Pt^{II}–Au^{I}} pair.

Cyanido transition metal complexes can also serve as effective metalloligands for constraining the coordination sphere of attached Ln(3+) ions towards substantial magnetic anisotropy, which follows a more general strategy of generating the Ln-SMMs *via* the insertion of 4f metal ions into coordination polymers and metal–organic frameworks.[101,220,221] The cyanido complexes can ensure the coordination skeleton for trapping the 4f metal ions, while the further optimization of magnetic anisotropy can be achieved by the supporting organic ligands. Simultaneously, the polycyanidometallate ions used for Ln-SMMs are usually diamagnetic. This provides good magnetic isolation of the 4f metal centres in the crystal lattice, weakening the magnetic interactions that can disturb the SMM properties of the Ln(III) centre. The Ln-geometry-constraining role of polycyanidometallates can be exemplified *via* our report on the application of *cis*-dicyanidoferrate(II) complexes with 2,2′-bipyridine (bpy) or 1,10′-phenanthroline (phen) co-ligands, which were combined with Dy^{3+} ions in the cyanido-bridged chains built using vertex-sharing {$Dy^{III}_2Fe^{II}_2$} squares, *i.e.*, {$Dy^{III}(MeOH)_4[Fe^{II}(CN)_2(L_{NN})_2]_2$}$(CF_3SO_3)_3$·5MeOH ($L_{NN}$ = phen or bpy; Fig. 7a and b).[102] In these chains, the cyanido ligands constrain the equatorial plane of the embedded 4f metal ions. This enables the insertion of pyridine N-oxide (pyNO) ligands at the positions axial to the Dy^{III} centre, leading to the modified material {$Dy^{III}(pyNO)_2(MeOH)_2[Fe^{II}(CN)_2(L_{NN})_2]_2$}$(CF_3SO_3)_3$·1.5MeOH ($L_{NN}$ = phen or bpy). As the Dy^{III} centre reveals an oblate-type 4f metal electron distribution for the favoured highest m_J state (Fig. 3), the introduction of pyNO ligands induces significant magnetic anisotropy and the SMM properties. The indirect but critical influence of the cyanido metal complexes on the slow magnetic relaxation of Ln-SMMs has been presented by us for the family of supramolecular networks based on $[Yb^{III}$(2,2′-bipyridine-1,1′-dioxide)$_4]^{3+}$ complexes.[222] They crystallize with various cyanido- and thiocyanido-metallate counter-ions which modulate the SMM characteristics, including the parameters of Raman and QTM processes (Fig. 7c and d). We also found that the Yb(III) complexes exhibit NIR luminescence. The related detailed emission pattern and the emission sensitization were found to be influenced by the applied cyanido metal complex. Moreover, from *ab initio* calculations, we were able to indicate the easy-axis-type ground doublets for the Yb^{III} centres formed in this family of compounds. Despite their differences in magnetic axiality, the transversal *g*-tensor components are always large enough to explain the lack of zero-dc-field relaxation. In every case, the excited doublets lie more than 120 cm^{-1} above the ground doublet, which was confirmed *via* high-resolution emission spectra that were also reproduced using *ab initio* calculations, giving a reliable insight into the energies and oscillator strengths of optical transitions. Therefore, we showed that polycyanidometallate can influence the magneto-luminescence properties of emissive Ln-SMMs, even without a direct coordination bond through the cyanido bridge, and the *ab initio* theoretical approach can greatly contribute to the elucidation of these effects as well as enabling their future optimization.

From the above view, one can notice that cyanido metal complexes can ensure the appropriate coordination environment

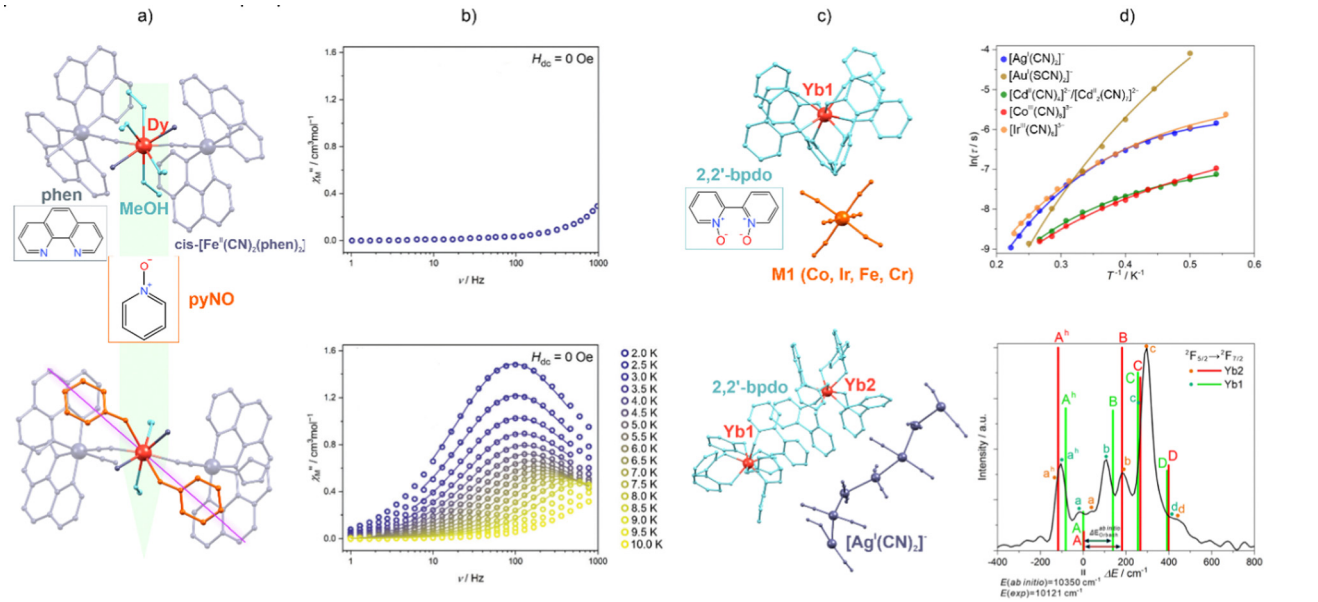

Fig. 7 (a) Structural views of {$Dy^{III}(MeOH)_4[Fe^{II}(CN)_2(L_{NN})_2]_2$}$(CF_3SO_3)_3$·5MeOH (top) and {$Dy^{III}(pyNO)_2(MeOH)_2[Fe^{II}(CN)_2(L_{NN})_2]_2$}$(CF_3SO_3)_3$·1.5MeOH (bottom) ($L_{NN}$ = 2,2′-bipyridine, 1,10′-phenanthroline; pyNO = pyridine N-oxide),[102] and (b) their temperature-variable ac magnetic characteristics of under zero dc magnetic field. (c) Structural views of the supramolecular frameworks built of $[Yb^{III}$(2,2′-bipyridine-1,1′-dioxide)$_4]^{3+}$ and indicated polycyanidometallate ions,[222] and (d) their respective temperature-variable magnetic relaxation times fitted using the contributions from Raman, direct and QTM processes (top), as well as the high-resolution emission spectra for the $[Ag^{I}(CN)_2]^-$-based analogue shown with the cumulative oscillator strengths (coloured bars) determined through *ab initio* calculations (bottom). Part (b) was reproduced from ref. 102 with permission from the Royal Society of Chemistry. Part (d) was adapted from ref. 222 which was published under the ACS AuthorChoice license.

of Ln(3+) ions to induce both luminescence and SMM properties. We showed this for the first time in 2016 when a white-light-emissive Dy(III) molecular nanomagnet, formed within Ln-hexacyanidocobaltate(III) chains, was presented.[101] More recently, combining Dy(III) complexes with O-donor 4-pyridone ligands and hexacyanidometallates of Co^{III} and Rh^{III}, we obtained dinuclear molecules of $\{[Dy^{III}(4\text{-pyridone})_4(H_2O)_2][M^{III}(CN)_6]\}\cdot nH_2O$ (Fig. 8a and d).[223] They show excitation-wavelength-dependent yellow-to-blue luminescence, as well as near-white-light emission of the improved characteristics appearing upon Co-to-Rh substitution. Moreover, both compounds exhibit strong Dy(III) magnetic anisotropy, leading to SMM properties. Analogously to the luminescence, the SMM features are enhanced *via* the change from {DyCo} to {DyRh} molecules, as shown, for example, in the increase in the anisotropic energy barrier from 187(6) K to 214(4) K, respectively.

A special type of Ln(III)-emission sensitization has been presented in other heterometallic d–f coordination networks, *i.e.*, $(PPN)[Ln^{III}(pzdo)_2(MeOH)_{0.3}(H_2O)_{3.7}][M^{IV}(CN)_8]\cdot 7.7H_2O\cdot 2MeOH$ (Ln = Er, Yb; M = Mo, W; pzdo = pyrazine *N*,*N*′-dioxide; PPN = bis(triphenylphosphine)iminium; Fig. 8b and e).[224] We showed that, owing to the strong visible-light absorption that is related to the series of electronic transitions assignable to the pzdo ligands and $[M^{IV}(CN)_8]^{4-}$ ions, as well as the appearance of a low-energy anion–π CT band involving pyrazine rings and cyanido ligands, the NIR emission of the Er(III) and Yb(III) centres is efficiently sensitized. Moreover, the related energy transfer is highly dependent on the d-metal centre in the $[M^{IV}(CN)_8]^{4-}$ ion. The W^{IV} centre was found to be a better sensitizer for Er^{III} whereas Mo^{IV} is preferred for Yb^{III} emission, which was explained by the suitable energy positions of the respective CT-donor electronic states. Both Er(III)- and Yb(III)-based analogues exhibit field-induced slow magnetic relaxation that originates from the equilibrium between QTM, direct, and Raman processes. The scheme of the relaxation routes is affected by the transition metals, which subtly change the coordination sphere of the Ln(III) centre, modifying also the phonon modes that govern the Raman relaxation. Even highly-structured three-dimensional cyanido-bridged frameworks can be employed as an advanced ligand for the generation of emissive Ln-SMMs. This was shown by us in the three-dimensional coordination networks $[Ln^{III}(2,2'\text{-bpdo})_2(H_2O)]$ $[Cu^{I}_2(CN)_5]\cdot 5H_2O$ (Ln = Dy, Yb; 2,2′-bpdo = 2,2′-bipyridine *N*,*N*′-dioxide; Fig. 8c and f).[225] Owing to the two

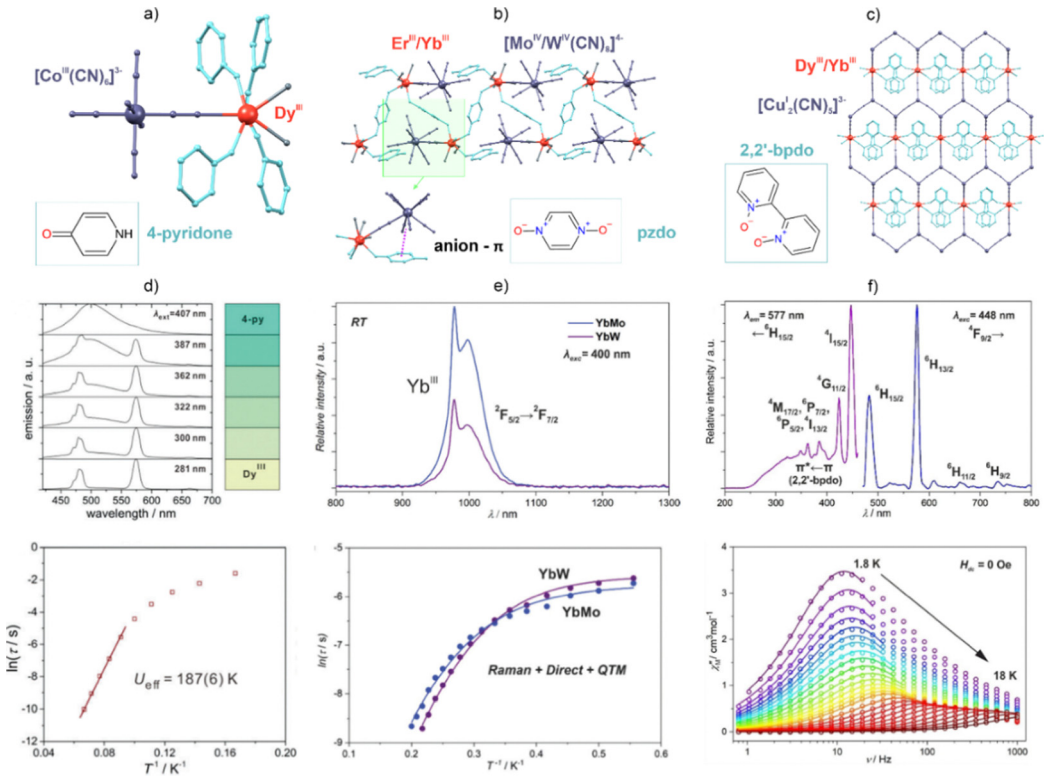

Fig. 8 (a) Structural view of the $\{[Dy^{III}(4\text{-pyridone})_4(H_2O)_2][Co^{III}(CN)_6]\}\cdot nH_2O$ dinuclear molecule (where an analogous structure is observed for the Rh^{III}-based derivative),[223] and (d) its excitation-wavelength-dependent emission spectra with the depicted emission colours (top), shown together with the temperature-variable magnetic relaxation times for the zero-dc-field (bottom). (b) Structural view of the $(PPN)[Ln^{III}(pzdo)_2(MeOH)_{0.3}(H_2O)_{3.7}][M^{IV}(CN)_8]\cdot 7.7H_2O\cdot 2MeOH$ coordination chains (Ln = Er, Yb; M = Mo, W; pzdo = pyrazine *N*,*N*′-dioxide; PPN = bis(triphenylphosphine)iminium),[224] and (e) the emission spectra for the related {YbMo} and {YbW} chains (top) shown together with the temperature-variable magnetic relaxation times for these compounds (bottom). (c) Structural view of the $[Ln^{III}(2,2'\text{-bpdo})_2(H_2O)][Cu^{I}_2(CN)_5]\cdot 5H_2O$ coordination networks (Ln = Dy, Yb; 2,2′-bpdo = 2,2′-bipyridine *N*,*N*′-dioxide; view of the layered part of the network),[225] and (f) the excitation and emission spectrum of the {DyCu} framework at 77 K (top), and its representative ac magnetic characteristics (bottom). Part (d) was reproduced from ref. 223 with permission from the Royal Society of Chemistry. Part (e) was reproduced from ref. 224 with permission from the Royal Society of Chemistry. Part (f) was adapted with permission from ref. 225. Copyright 2019 John Wiley & Sons.

axially-positioned 2,2′-bpdo ligands and the use of flexible polycyanidocuprate(I) anions, the obtained networks exhibit pronounced SMM properties for the {DyCu} analogue, which co-exists with its yellow Dy(III)-centred photoluminescence. Magneto-luminescent properties were also found for the {YbCu} network.

3. Stimuli-responsive luminescent lanthanide molecular nanomagnets

Molecule-based materials offer the possibility of controlling their physical properties, including the magnetic, optical, mechanical, or electrical properties, using external stimuli, *e.g.*, solvents or other chemicals, temperature, light, pressure, and magnetic or electric fields.[115–129,226–228] The switching of the physical effects *via* external stimuli can either lead to bi- or multi-state systems that are attractive, for example, in data storage applications,[229,230] or produce continuous large changes in the specific characteristics, even with a weak external factor, which is utilized in sensing applications.[231,232] Moreover, external stimuli can be employed for the generation or optimization of the desired properties, including luminescence functionalities as well as SMM and other magnetic effects, for the molecular systems, including those based on Ln(III) complexes.[127,233,234] Here, we will discuss representative examples of how external stimuli are used to switch, generate, or modulate the magnetic and luminescence properties of emissive Ln-SMMs, with the emphasis given to our contribution to this emerging research trend.

3.1 Chemical switching of luminescent lanthanide SMMs

Ln(III)-based coordination systems can be sensitive to chemical stimuli, including the exchange of solvent molecules which can often change the physical properties without the crystallinity of the material being lost.[117–119,126,233,235–239] Such removal or exchange of solvent molecules can modify the coordination environment of 4f metal ions, then both their luminescence and SMM properties are expected to be strongly modulated as they are directly related to the geometry and composition of the first coordination sphere of the Ln(III) centre.[82,83,191] Using a more subtle approach, the chemical treatment of a Ln(III)-based coordination compound may involve a non-coordinated solvent or other guest molecules that can affect the magneto-luminescent character by influencing, for example, the emission sensitization pathways or the phonon mode scheme that is important for Raman magnetic relaxation.[119,240,241] All of these perspectives have been explored separately in the fields of Ln(III)-based luminophores and Ln-SMMs,[126,233,235–239] although the chemical switching of emissive Ln-SMMs is very rare.[242] In this context, using the heterometallic approach based on polycyanidometallates (see Section 2.4), we prepared dinuclear molecules of $\{[Dy^{III}(H_2O)_3(2\text{-pyrrolidone})_4][Co^{III}(CN)_6]\}\cdot nH_2O$, which exhibit two stable crystalline phases with different amounts of water of crystallization (Fig. 9).[243] These two phases, *i.e.*, LH (low-humidity) and HH (high humidity), are interconverted upon variation of the relative humidity (RH). Moreover, there is a unique RH range of phase bistability where both crystalline phases co-exist.

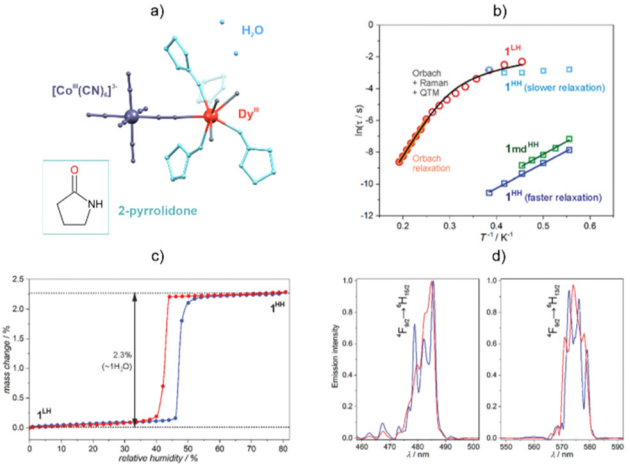

Fig. 9 (a) Structural view of the $\{[Dy^{III}(H_2O)_3(2\text{-pyrrolidone})_4][Co^{III}(CN)_6]\}\cdot nH_2O$ molecule,[243] (b) temperature dependence of magnetic relaxation times for the low- (LH) and high-humidity (HH) phases, (c) isotherm for water adsorption, and (d) emission spectra for 350 nm excitation. Parts (b–d) were adapted from ref. 243 with permission from the Royal Society of Chemistry.

The embedded Dy(III) centres reveal field-induced SMM properties for both phases; however, the single-crystal-to-single-crystal transformation from the HH to the LH phase results in a significant slowdown of the magnetic relaxation and a three-fold increase in the efficient anisotropic thermal energy barrier. Moreover, this partial dehydration process influences the almost white-light Dy(III)-centred photoluminescence of the LH phase, effectively shifting its colour to yellow. We expanded this idea of the chemical tuning of emissive Ln-SMMs by combining similar molecular building blocks, namely, Dy^{3+} and hexacyanidocobaltate(III) ions, but in the absence of organic ligands.[207] We obtained a three-dimensional cyanido-bridged framework, $\{[Dy^{III}(H_2O)_2][Co^{III}(CN)_6]\}\cdot 2.2H_2O$, that can be reversibly dehydrated, subsequently adopting the form of $\{Dy^{III}[Co^{III}(CN)_6]\}$ (Fig. 10). This

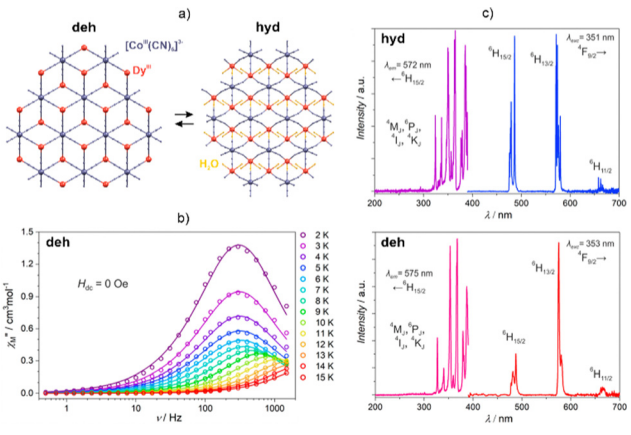

Fig. 10 (a) Structural view of three-dimensional $\{[Dy^{III}(H_2O)_2][Co^{III}(CN)_6]\}\cdot 2.2H_2O$ (hyd) and $\{Dy^{III}[Co^{III}(CN)_6]\}$ (deh) networks,[207] (b) representative ac magnetic characteristics of the deh phase, and (c) excitation and emission spectra at 77 K for both the hyd (top) and deh (bottom) phases (c). Parts (b and c) were adapted with permission from ref. 207. Copyright 2019 American Chemical Society.

single-crystal-to-single-crystal transformation results in a dramatic change of the Dy(III) coordination geometry from square-antiprismatic to trigonal prismatic, which leads to the generation of Dy(III) SMM behaviour as the hydrated phase does not exhibit slow magnetic relaxation. The Dy(III)-centred photoluminescence is also affected by dehydration, as the emission colour essentially shifts from nearly-white to deep-yellow. This change was assigned to modulation of the details of the emission bands due to modification of the symmetry of the Dy(III) complexes.

3.2 Optical thermometers based on luminescent lanthanide SMMs

A highly sensitive optical response to temperature variation, which can be realized *via* luminescence, *e.g.*, the emission colour, emission band intensity, or emission lifetime, is one of the desired functionalities in modern materials science.[68,155,244–246] Ln(III)-containing molecular materials, including molecular systems and coordination polymers, have been found to be efficient for the construction of high-performance luminescent thermometers, especially those that show ratiometric character where the crucial thermometric parameter consists of the ratio between two distinct emission features, *e.g.*, the emission intensities of separate molecular components (see Section 2.1).[68,155] Such ratiometric luminescent thermometers provide a convenient route for contactless temperature sensing in various devices as they offer high sensitivity that is independent of the experimental setup, in contrast to, for example, the overall emission intensity. In general, to achieve good luminescent thermometry, the material must show a high relative thermal sensitivity (S_r) coupled with a low temperature uncertainty (δT) in a maximally broad temperature range or the temperature range of interest. The limits of $S_r > 1\%\ K^{-1}$ and $\delta T < 1$ K indicate a good thermometric performance.[68,155,246]

The combination of luminescent thermometry with molecular nanomagnetism can not only provide a multifunctional material with co-existing optical and magnetic properties but also result in an advanced SMM, revealing the self-monitoring of its temperature using the optical response.[199] To achieve this, the optical thermometry must appear within the working range of the SMM properties, which itself signals another alternative of the correlation between the nanomagnetic character and temperature sensing as well as a pathway towards the possible influence of a magnetic field on the optical thermometry for a molecular nanomagnet (see Section 2.3).[147,199] Realizing such a temperature overlap between the optical thermometry and the single-molecule magnetism is a non-trivial task, since the slow magnetic relaxation for the current SMMs is usually observed to be well below the boiling nitrogen temperature where optical thermometry is often limited. However, adopting optimistic attitudes, we and other groups took on the challenge of constructing luminescent thermometers based on Ln-SMMs. Typical selection of the Ln(3+) ion consists of the exploration of yellow emissive Dy(III) or NIR-emissive Yb(III) centres for which the design of SMMs has broadly been recognized (see Section 2.2). For these candidates, optical thermometry was achieved, by us and other groups, by tracing the temperature variation of the detailed emission pattern where thermal depopulation of the m_J levels, including those responsible for the strongly temperature-dependent hot bands, is observed.[83,198,247–250]

In our work, we searched for non-trivial approaches to achieve optical thermometry in Ln-SMMs constructed using cyanido metalloligands. We obtained dinuclear molecules, $\{[Ho^{III}_{x}Y^{III}_{1-x}(4\text{-pyridone})_4(H_2O)_2][M^{III}(CN)_6]\}\cdot nH_2O$ (M = Co, Rh, Ir), where the Ln position is occupied by Ho(III) or Y(III). They revealed the SMM effect, originating from the pentagonal bipyramidal Ho(III) complexes (Fig. 11).[251] More interestingly, owing to Y^{III}-based dilution, the material shows room-temperature, blue, 4-pyridone-centred emission, which was not observed in the Y(III)-free analogue, due to the dominant Ho(III) re-absorption process. However, for the Y(III)-diluted samples, we reported sharp re-absorption peaks within the ligand's emission band. The luminescence re-absorption effect was assigned to the specific ladder-type electronic structure of Ho(III),[252] and it was found to depend strongly on the temperature. Thus, we utilized the ratios between selected re-absorption band intensities as thermometric parameters, achieving ratiometric optical thermometers with a good performance that ranged from ~25 to 205 K. We were also able to tune the thermometric effect through d-metal ion substitution within the hexacyanidometallate complex. In this work, we proved that luminescence thermometry based on Ln-SMM can be achieved by exploring the organic ligand emission with the support of the luminescence re-absorption effect.

Recently, the further expansion of the concept of optical thermometry using emissive Ln-SMMs was presented.[253] For the

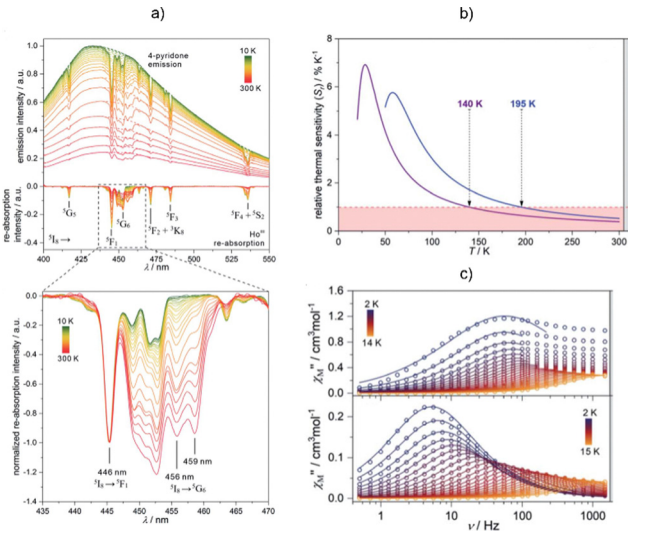

Fig. 11 (a) Temperature-dependent emission spectra of $\{[Ho^{III}_{0.11}Y^{III}_{0.89}(4\text{-pyridone})_4(H_2O)_2][Co^{III}(CN)_6]\}\cdot nH_2O$ molecules (which are isostructural to the {DyCo} molecules shown in Fig. 8a) measured under 370 nm excitation together with the extracted luminescence re-absorption spectra obtained after subtraction of the ligand emission component, (b) resulting temperature dependence of the relative thermal sensitivity for two different ratios of luminescence re-absorption peaks, and (c) representative ac magnetic characteristics (top) compared with the undiluted sample (bottom). Reproduced from ref. 251 with permission from the Royal Society of Chemistry.

first time, a combination of the thermometric effects using Raman spectroscopy and photoluminescence was reported. This was shown for novel supramolecular assemblies of $\{[Dy^{III}_{x}Y^{III}_{1-x}(phen)_2(\mu\text{-}OH)_2(H_2O)_2]\}[Au^{I}(SCN)_2]_2\cdot phen\cdot 0.5MeCN\cdot 0.5H_2O$ (x = 0, 0.1, 0.02; phen = 1,10′-phenanthroline) that feature weakly bonded Ln(III) and Au(I) metal complexes (Fig. 12). They exhibit Raman scattering in the low-frequency regime with sharp peaks. Three vibrational bands were selected to exploit the related thermometric behaviour, revealing good sensitivity in the low-temperature region, comparable to the simultaneously found luminescent thermometry based on the temperature variation of the Dy(III)-centred emission pattern. It was suggested that the low-frequency phonons related to the {Au–Au} vibrations increase the thermometric sensitivity of both types of detected optical thermometer. The applicability of the thermometric effect based on the Raman effect in various solvents was demonstrated. Finally, owing to the presence of Dy(III) centres, additionally diluted with Y(III) centres, the SMM properties were detected and also correlated with the low-energy vibrational modes that are detectable in Raman spectroscopy.

3.3 Photo-switching of luminescent lanthanide SMMs

The use of light stimuli to affect the SMM behaviour and modulate the luminescence properties has a wide spectrum of potential applications, for optical switches as well as information-storage and -processing devices, which has separately been proved in the families of photochromic luminophores and photomagnetic materials.[103,104,123–125,128] The simultaneous photo-switching of both emission and magnetism is expected to enrich the physical response from the sample and open a route for the photo-control of possible magneto-luminescence coupling effects.

Achieving photoswitchable luminescent SMMs is a tremendous challenge as most of the photosensitive molecular building blocks used for molecular photomagnets hamper the emission properties. This occurs since many photoswitchable organic ligands, as well as metal complexes, *e.g.*, spin-crossover-active Fe(II) and Mn(III) centers, and pairs of metal complexes that show photoinduced electron transfer, *e.g.*, cyanido-bridged Co(II) and W(V) or Co(II) and Fe(III) centers, are strongly coloured, which limits their emission properties.[103,104,107,109] Moreover, the light must be used to switch the state of the system, and it must be ensured that light of a different wavelength simultaneously induces luminescence without changing the state of the material. A few research groups have addressed this challenge using luminescent Ln-SMMs.[129,254–258] They mainly explored a strategy that relies on the incorporation of photo-responsive organic components into the system, which, through photo-chemical reactions, causes structural changes that affect both luminescence and magnetic properties. Wang *et al.* reported a family of coordination-chain-based supramolecular compounds, $[Ln^{III}_3(H\text{-}HEDP)_3(H_2\text{-}HEDP)_3]\cdot 2(H_3\text{-}TPT)\cdot(H_4\text{-}HEDP)\cdot 10H_2O$ (Ln = Dy, Gd, Y; HEDP = hydroxyethylidene diphosphonate; TPT = 2,4,6-tri(4-pyridyl)-1,3,5-triazine), that exhibit reversible room-temperature photochromism (both in absorption and emission) and photomagnetism (Fig. 13).[129] Moreover, the Dy^{III}-based analogue, QDU-1(Dy), shows zero-dc-field SMM behaviour after UV-light-induced phototransformation. The above features are related to the occurrence of photoinduced electron transfer (PET), resulting in the photogenerated radicals $TPT^{\bullet}$ and $O^{\bullet}$. For QDU-1(Dy), the initially colourless sample becomes blue upon UV-light irradiation. The time-dependent fluorescence spectra indicate that the intensity of the TPT fluorescence decreases upon UV-light irradiation. This fluorescence quenching was rationalized through the conversion of the fluorescent H_3-TPT components to non-fluorescent $TPT^{\bullet}$ radicals. It is worth mentioning that the photo-generation of radicals entails structural changes, leading to unit cell shrinkage. Structural variations also include strengthening of the H-bonding network and decreasing the N···O distance between the HEDP-Ln moiety and the TPT ligand. Furthermore, QDU-1(Dy) exhibits a light-induced SMM effect owing to the appearance of ferromagnetic coupling between the Dy^{3+} ions and $O^{\bullet}$ radicals. Thus, QDU-1(Dy) constitutes a unique example of a photochromic switch, in which the slow relaxation of magnetization can be generated by light stimuli.

Other examples of photoswitchable Ln-SMMs have been presented by Zheng and co-workers.[255,257] First, they obtained the mono-nuclear Dy(III) complexes bearing the 9-diethylphosphonomethylanthracene (depma) ligand that undergo reversible [4+4] photodimerization leading to a change in the SMM effect and a switch from yellow-green to blue-white emission.[257] Furthermore, they enhanced the multifunctionality to obtain a remarkable molecular material, enabling the synergistic switching of its luminescence, magnetic, and dielectric properties using thermo- and light-stimuli. The reported Dy^{III} complex, $[Dy^{III}(SCN)_3(depma)_2(4\text{-pyridone})_2]$, contains depma and 4-pyridone ligands, which play the roles of photo-active and polar components,

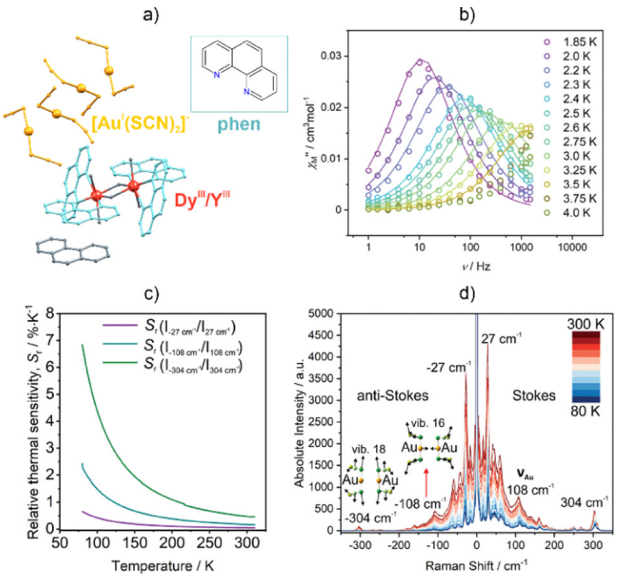

Fig. 12 (a) Structural view of the $\{[Dy^{III}_{x}Y^{III}_{1-x}(phen)_2(\mu\text{-}OH)_2(H_2O)_2]\}[Au^{I}(SCN)_2]_2\cdot phen\cdot 0.5MeCN\cdot 0.5H_2O$ supramolecular assemblies (x = 0, 0.1, 0.02; phen = 1,10′-phenanthroline),[253] (b) representative ac magnetic characteristics for the x = 0.02 sample, (c) temperature dependence of the relative thermal sensitivity for the three indicated ratios of peaks in the Raman spectra, and (d) Raman spectra of the x = 0 sample at the temperatures shown, as used for (c). Parts (b–d) were adapted from ref. 253 under the terms of the Creative Commons CC BY license.

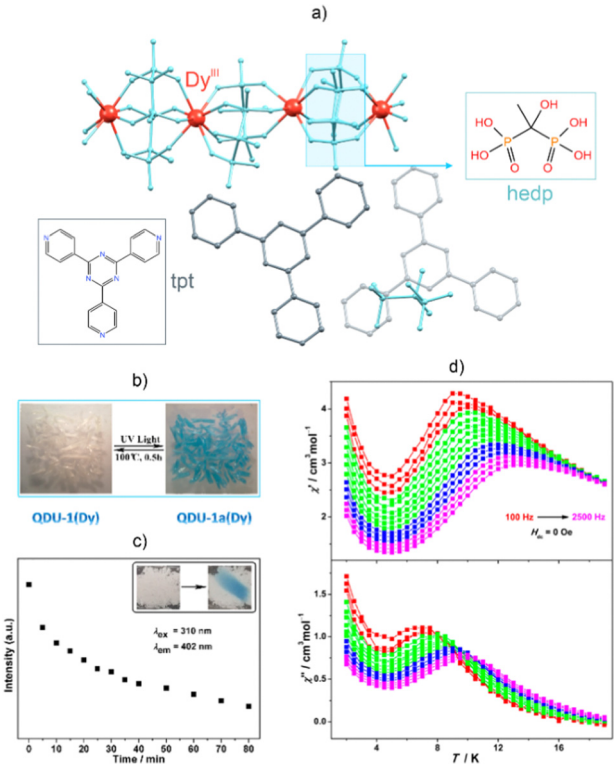

Fig. 13 (a) Structural view of the $[Dy^{III}_3(H\text{-}HEDP)_3(H_2\text{-}HEDP)_3]\cdot 2(H_3\text{-}TPT)\cdot(H_4\text{-}HEDP)\cdot 10H_2O$ supramolecular framework (QDU-1(Dy)) (HEDP = hydroxyethylidene diphosphonate; TPT = 2,4,6-tri(4-pyridyl)-1,3,5-triazine),[129] (b) its reversible photochromic behaviour, (c) the irradiation-time dependence of the fluorescence intensity of the TPT ligand, and (d) the temperature dependence of the χ' (top) and χ'' (bottom) components of the ac magnetic susceptibility for the UV-light-irradiated QDU-1a(Dy) sample. Parts (b–d) were adapted with permission from ref. 129. Copyright 2020 American Chemical Society.

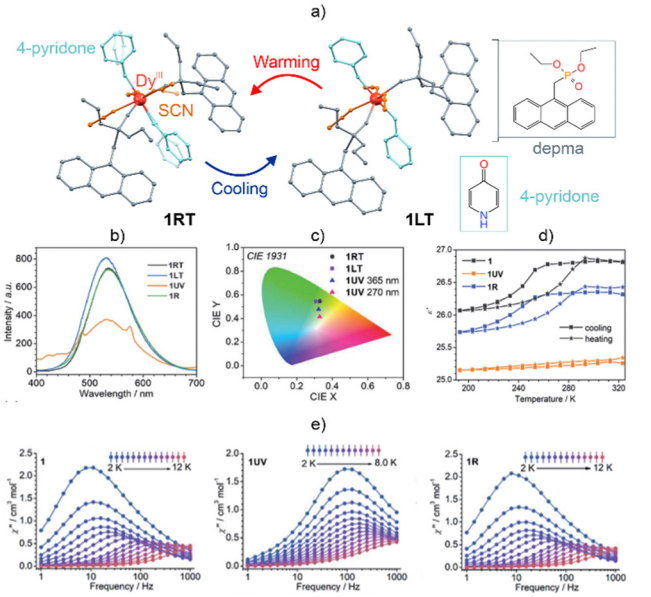

Fig. 14 (a) Structural transformation of the $[Dy^{III}(SCN)_3(depma)_2(4\text{-pyridone})_2]$ complex *via* the transition from a high-temperature (1RT) to a low-temperature (1LT) phase,[255] (b) emission spectra under the 365 nm excitation for 1RT and 1LT as well as the photo-dimerized phase (1UV) and the product obtained after reversing the dimerization process (1R), (c) related emission colours on the CIE 1931 chromaticity diagram, (d) temperature dependence of the dielectric constant for 1(LT/RT), 1UV, and 1R at the frequency of 1328 kHz, and (e) representative ac magnetic characteristics for 1 (LR/RT) (left), 1UV (middle), and 1R (right). Reproduced from ref. 255 with permission from the Royal Society of Chemistry.

respectively (Fig. 14).[255] The thermo-responsivity of this material is linked to the phase transition between the high- and low-temperature phases (named 1RT and 1LT, respectively) that occur due to the order–disorder transition of the 4-pyridone and SCN^- molecular components. This reversible phase transition manifests as a noticeable change in the emission characteristics. The temperature has a large impact on the dielectric properties, and this effect is correlated with the local dynamic changes of the polar components. Moreover, due to the occurrence of photo-induced dimerization involving the anthracene groups of the depma ligands, the system is highly responsive to light stimuli. The UV-light stimulus leads to a considerable structural transformation that is accompanied by a change in the luminescent properties. One can observe a decrease in the 535 nm ligand-centered emission peak intensity and, at the same time, the appearance of additional distinct bands that are ascribed to the π^*–π transitions of dianthracene moieties and f–f electronic transitions of Dy^{3+} ions. This suggests the light-induced modification of the ^{3}T ligand state energy and an enhancement of the sensitization of the Dy^{III}-based emission. Moreover, the photo-dimerization reaction leads to a reduction in the relative permittivity, ε', and the quenching of its thermally induced dielectric transition. The light stimulus also influences the magnetic properties, affecting the shape of the magnetic hysteresis loop and shifting the peaks in the $\chi''(\nu)$ curves towards higher frequencies. This observation was rationalized by the symmetry lowering around the Dy^{3+} ion that is caused by the photocycloaddition reaction. Therefore, this material shows an unprecedented synchronous modulation of three various functionalities embedded into a single-phase material based on a luminescent Dy-SMM.

4. Electrical functionalities generated in luminescent lanthanide molecular nanomagnets

The electrical properties, including the high ionic (*e.g.*, proton or alkali ion) or electronic conductivity, superconductivity, pyro-, piezo-, and ferroelectricity, have aroused continuous interest in materials science.[259–262] Their combination with luminescence as well as the magnetism in multifunctional materials has also been broadly recognized due to the attractive electro-optical and magneto-electric phenomena that can be produced.[20–23,263,264] Using the molecular building block approach, the conjunction of electrical and luminescent or magnetic effects, including SMM properties, has been found. For instance, luminescent molecular ferro-electrics or electron conductive SMMs have been prepared.[32,33,265,266] Among them, Ln(III)-based materials were also presented, opening a route to

the generation of electrical functionalities in the coordination of supramolecular frameworks based on emissive Ln molecular nanomagnets.[265–269] In this section, we will briefly discuss the pioneering studies on such advanced multifunctional systems that link luminescent and SMM properties with electrical effects, mainly proton conductivity and ferroelectricity.

4.1 Proton conductivity in molecule-based materials incorporating lanthanide SMMs

The design and synthesis of solid proton-conducting materials continues to be a major challenge faced in the areas of green chemistry and sustainable engineering. Proton conductors give hope for new solutions in the field of clean energy, since they are a key component in the process of energy conversion in fuel cells and other hydrogen-focused technological innovations.[259,270,271] In this context, metal–organic frameworks (MOFs) have remained in the spotlight and have commonly been investigated owing to their adjustability, which enables the incorporation of proton pathways into their frameworks.[259,267,272] Heterometallic cyanido-bridged systems have also been recognized as attractive in these regards, especially taking into consideration the possibility of combining a high proton conductivity with other functionalities, in particular, magnetic functionalities.[273–275] We found that metal cyanido complexes can be suitable for the synthesis of Ln-SMMs that exhibit this highly demanded electrical property. We reported the generation of both a high proton conductivity and luminescent thermometry in the emissive supramolecular network of $(H_5O_2^+)_2(H^+)[Yb^{III}(hmpa)_4][Co^{III}(CN)_6]_2{\cdot}0.2H_2O$ (hmpa = hexamethylphosphoramide; Fig. 15).[247] This unique system shows unprecedented multifunctionality, operating as a proton conductive luminescent thermometer based on NIR-emissive SMMs. The embedded Yb(III) complexes exhibit slow relaxation of magnetization below 6 K as the result of using O-donor ligands that occupy the equatorial positions around the 4f metal ion. Moreover, the Yb(III) centres exhibit room-temperature NIR photoluminescence that is sensitized by the $[Co^{III}(CN)_6]^{3-}$ ions. The related luminescent thermometric functionality was also observed. It is related to the non-trivial application of the strongly temperature-dependent hot emission bands and complex temperature variation of main emission peaks observed at 975 and 1020 nm. Aside from the optical and magnetic properties, the multifunctional nature of the obtained material was extended to proton conductivity, which appears due to the presence of dihydronium ions in the form of $H_5O_2^+$ within its crystal structure. At 30% RH (relative humidity), the electrical conductivity related to the proton motion, σ, was determined to be low, reaching 1.5×10^{-9} S cm^{-1}. However, the conductance was found to be strongly sensitive to the humidity variation. At higher RH levels, one can observe a rapid increase of the σ value to a maximum of 1.7×10^{-4} S cm^{-1} at 97% RH, which can be ascribed to superionic conductor behaviour. According to the temperature-variable impedance spectra and the course of the $\ln(\sigma T)$ *versus* T^{-1} dependence, proton conduction is postulated to operate through the Grotthuss mechanism, as suggested by the value of the activation energy (E_a = 0.44(1) eV) extracted from experimental data using the Arrhenius law. In the postulated mechanism, proton transport occurs through the channels aligned with the *c* crystallographic axis which, at higher values of RH, are occupied by water molecules, weakly interacting with the N-atoms of the hmpa ligands. Such a columnar porous framework provides an advantageous pathway for the proton hopping mechanism that involves H-containing

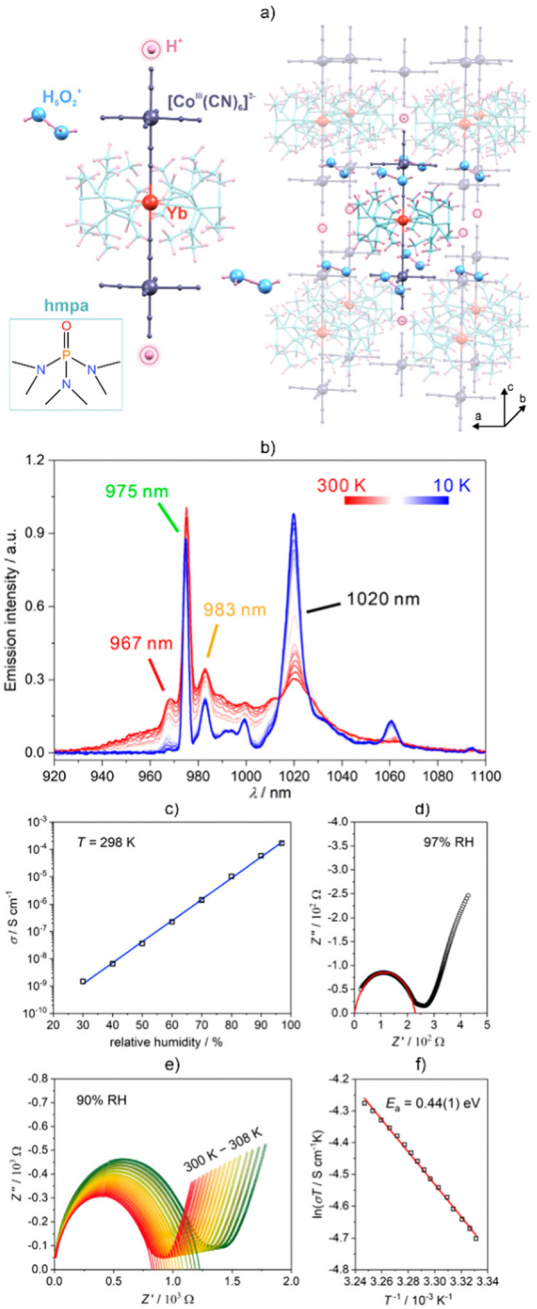

Fig. 15 (a) Crystal structure of the $(H_5O_2)_2(H)[Yb^{III}(hmpa)_4][Co^{III}(CN)_6]_2{\cdot}0.2H_2O$ molecule-based material (hmpa = hexamethylphosphoramide),[247] (b) temperature-variable emission spectrum under 320 nm excitation, (c) humidity dependence of the electrical conductance, (d) the related impedance spectrum at 97% RH, (e) temperature-variable impedance spectra at 90% RH (e and f) the related Arrhenius plot with the indicated activation energy. Parts (b–f) were adapted with permission from ref. 247. Copyright 2020 American Chemical Society.

cations, generating superionic conductivity in the described system.

Some other research groups have also recently presented unique examples of proton conductive materials based on luminescent Ln-SMMs. Among them, the supramolecular approach that utilizes weak intermolecular interactions, similar to our findings, was explored, while other routes take advantage of the formation of Ln(III)-based MOFs with suitably selected organic linkers that ensure energy transfer for Ln(III)-emission sensitization, suitable magnetic anisotropy, and structural pores for proton conduction. In these approaches, the weakest point appeared to be the design of magnetic anisotropy since all of these reported proton-conductive emissive Ln-SMMs demonstrate only moderate slow magnetic relaxation characteristics.[276–278]

4.2 Ferroelectricity in molecule-based materials incorporating lanthanide SMMs

The generation of electrical properties related to switchable electric polarization, including pyroelectricity and ferroelectricity in particular, into magnetic materials, and also recently into molecule-based magnets, constitutes an emerging trend in materials science. Such advanced systems can potentially be used as multiferroic and magnetoelectric materials, enabling the modulation of electric polarization using a magnetic field, or the modulation of magnetic effects using an electric field.[36,37,279–281] Such magneto-electric phenomena have broad application horizons, *e.g.*, in memory devices or spintronics. Pioneering reports have shown that ferroelectricity can also be induced for SMMs, including those based on Ln(III) complexes.[130,282] By contrast, the analogous electrical properties, such as ferroelectricity, were combined with luminescence, which is a route for the effective manipulation of light emission using an electric field.[283,284] In particular, a group of luminescent molecular ferroelectrics – which are usually based on molecular perovskites – emerged, opening a new perspective for electro-optical coupling effects.[32,33] In these contexts, a broadened multifunctionality is expected in which ferroelectricity will appear for emissive Ln-SMMs, which will demand the generation of a suitable polar space group and the insertion of polar components that can induce the appearance of a spontaneous and further switchable electric polarization characteristic for ferroelectrics. This must be ensured together with the distinct luminescence and magnetic anisotropy of the Ln(III) complex.

Only a very few attempts at producing ferroelectric luminescent Ln-SMMs have been successful.[285–289] Among them, tremendous functional potential was uncovered by Long *et al.* who reported high-temperature ferroelectrics based on the chiral $[Zn^{II}(R,R\text{-L})Dy^{III}(\mu\text{-OAc})(NO_3)_2]$ (A-*R*,*R*-1) and $[Zn^{II}(S,S\text{-L})Dy^{III}(\mu\text{-OAc})(NO_3)_2]$ (A-*S*,*S*-2) complexes that exhibit Dy(III)-centred luminescence, natural optical activity, and slow magnetic relaxation (Fig. 16).[288] Molecular crystals of both enantiomers crystallize in the polar $P2_1$ space group and exhibit electrical polarization bistability up to 563 K, thus reaching one of the highest temperatures reported for molecular ferroelectric materials. Astonishingly, the crystal structure remains polar, and the crystallinity is preserved as well as the ordered structure up to the decomposition temperature of ~570 K. More recently, Long *et al.* presented a continuation of this research pathway.[289] They reported the magnetoelectric control of ferroelectric domains in analogous molecule-based materials. The molecules $[Zn^{II}(R,R\text{-L})Yb^{III}(\mu\text{-OAc})(NO_3)_2]$ (B-*R*,*R*-1) and $[Zn^{II}(S,S\text{-L})Yb^{III}(\mu\text{-OAc})(NO_3)_2]$ (B-*S*,*S*-2), just like the Dy(III)-containing predecessors, adopt the polar $P2_1$ space group and exhibit room-temperature ferroelectricity that co-exists with luminescence and SMM effects (Fig. 17). The ferroelectric transition temperature was estimated to be even higher than the decomposition temperature of these materials (~550 K). The obtained systems combine ferroelectricity with a magnetostrictive effect, generating a strong magnetoelectric coupling. It was found that a magnetic field of even down to 0.1 T can generate a significant mechanical strain through spin–lattice coupling, which simultaneously affects the electric polarization. Therefore, this unique molecular material exhibits the strongly desired magneto-electric coupling, which has broadly been explored in multiferroic metal oxides but is much less recognized for materials based on metal complexes.[290–293]

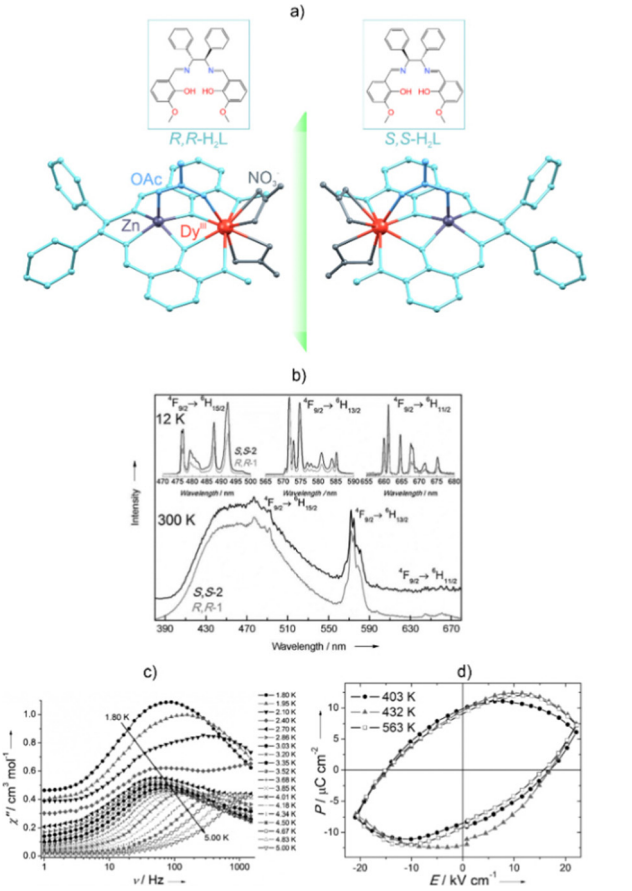

Fig. 16 (a) Crystal structures of the chiral molecular materials $[Zn^{II}(R,R\text{-L})Dy^{III}(\mu\text{-OAc})(NO_3)_2]$ (A-*R*,*R*-1) and $[Zn^{II}(S,S\text{-L})Dy^{III}(\mu\text{-OAc})(NO_3)_2]$ (A-*S*,*S*-2),[288] (b) their emission spectra under 365 nm excitation, (c) representative ac magnetic characteristics under a dc field of 1500 Oe for A-*R*,*R*-1, and (d) ferroelectric hysteresis loops at the indicated temperatures for A-*R*,*R*-1. Parts (b)–(d) were adapted with permission from ref. 288. Copyright 2015 John Wiley & Sons.

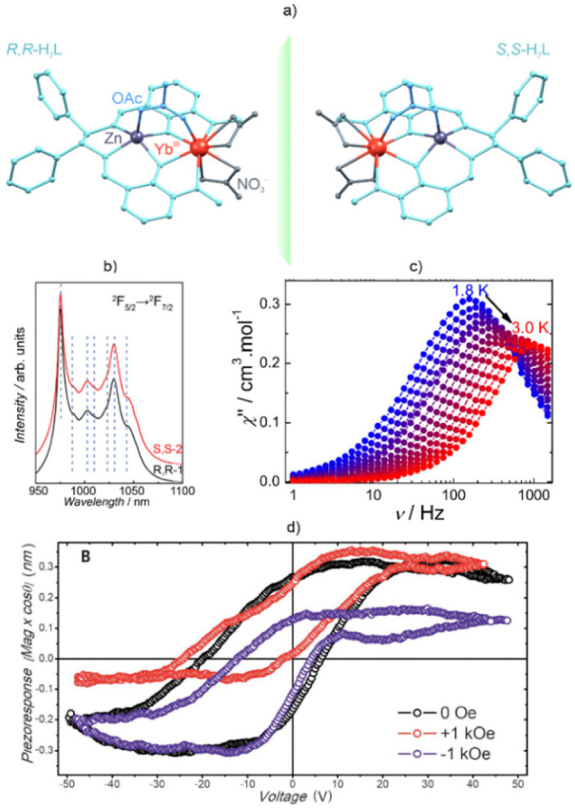

Fig. 17 (a) Structural view of the chiral molecules $[Zn^{II}(R,R\text{-L})Yb^{III}(\mu\text{-OAc})(NO_3)_2]$ (B-*R*,*R*-1) and $[Zn^{II}(S,S\text{-L})Yb^{III}(\mu\text{-OAc})(NO_3)_2]$ (B-*S*,*S*-2),[289] (b) their room-temperature NIR-emission spectra under 405 nm excitation, (c) representative ac magnetic characteristics under a dc field of 600 Oe for B-*R*,*R*-1, and (d) ferroelectric hysteresis loops under the indicated magnetic fields for B-*R*,*R*-1. Parts (b–d) were adapted with permission from AAAS, from ref. 289.

5. Non-centrosymmetricity- and chirality-related optical effects in luminescent lanthanide molecular nanomagnets

The other potential functionalization of emissive Ln-SMMs consists of introducing chirality. Functional solids that reveal a chiral or at least a non-centrosymmetric structure may potentially exhibit additional optical and magneto-optical properties. For instance, chiral magnets, including molecule-based magnets, can exhibit natural optical activity (NOA) that originates from broken spatial symmetry.[294,295] The corresponding effect of magnetic optical activity (MOA) can be generated even in centrosymmetric systems through the application of an external magnetic field, breaking the time-reversal symmetry.[295–297] If both types of symmetry are broken, the magneto-chiral dichroism (MChD) cross-effect may occur in which the absorbance investigated for the unpolarized light of a given chiral molecule is dependent on the direction of the magnetic field.[106,294,298] It has great application potential, *e.g.*, as the advanced optical output of magnetic data using unpolarized light. The MChD effect has been recognized in the family of chiral molecular magnets and some magnetic metal complexes; however, it has not yet been explored for Ln-SMMs.[299,300] This research trend is expected to emerge, as suggested by the report on chiral $[Yb^{III}((X)\text{-L})(hfac)_3]$ complexes (L = 3-(2-pyridyl)-4-aza[6]helicene; X = *P*, *M*; hfac = 1,1,1,5,5,5-hexafluoroacetylacetonate).[133] They show a significant MChD signal (an anisotropy factor, g_{MChD} of $\sim 0.12\ T^{-1}$) that is correlated with the $^2F_{7/2} \rightarrow {}^2F_{5/2}$ electronic transition of the Yb^{III} centre.

Furthermore, materials that crystallize in non-centrosymmetric space groups can also exhibit non-linear optical effects, *e.g.*, second harmonic generation (SHG).[301,302] The SHG phenomenon consists of the interaction of photons of the given frequency ω with a solid material that lacks inversion symmetry, giving rise to a frequency-doubling effect. SHG crystals are crucial for optoelectronic and laser technologies.[7,301] It has been shown that the SHG effect can be modulated using a magnetic field, especially when the SHG-active magnet is constructed. The related magnetization-induced SHG (MSHG) phenomenon can lead to a huge enhancement of the SHG in the magnetically ordered phase, and molecule-based magnets have been found to be very attractive for this application.[17,21] The SHG activity was successfully combined with luminescence in several types of material, especially in Ln(III)-based MOFs.[112,302] SHG-active molecular nanomagnets, including Ln(III)-based molecular magnets, have also been shown;[303] thus, the natural step was to focus on SHG-active luminescent Ln-SMMs, which will be discussed below. The combination of chirality and luminescence leads to the observation of CPL, which is related to the differential intensities of the left and right circularly polarized components of the emitted light.[304] CPL-active materials are now widely explored due to their prospective applications, *e.g.*, in 3-D displays or data storage,[305,306] and here we will discuss the pioneering studies regarding the generation of the CPL phenomenon in luminescent SMMs based on Ln(III) complexes.

5.1 Second-harmonic generation activity of acentric luminescent lanthanide SMMs

The generation of the SHG activity together with luminescence and SMM properties is expected to enrich the multifunctionality. It will also open a pathway for novel opto-magnetic coupling effects especially in the case when the SHG signal will be gathered for the high-performance SMM showing the magnetic memory effect at the sufficiently high temperature. Following these perspectives, we and other groups focused on the challenge to break the symmetry of the crystalline phases based on emissive Ln-SMMs to induce SHG activity.[276,307,308] While the other groups focused on enantiomeric organic ligands that ensure all of the necessary features, SHG-activity, luminescence, and magnetic anisotropy, we took advantage of the heterometallic approach that utilizes octacyanidometallate ions of Mo(IV) and W(IV) (Fig. 18).[308] We obtained layered coordination polymers, $\{[Nd^{III}_4(H_2O)_{17}(pzdo)_5][M^{IV}(CN)_8]_3\}\cdot 9H_2O$ (M = Mo, W; pzdo = pyrazine-*N*,*N*′-dioxide), based on cyanido and pzdo molecular bridges.[308] Owing to the spontaneous resolution process related to the unusual 3 : 4 metal ratio and anion–π interactions involving pzdo ligands and

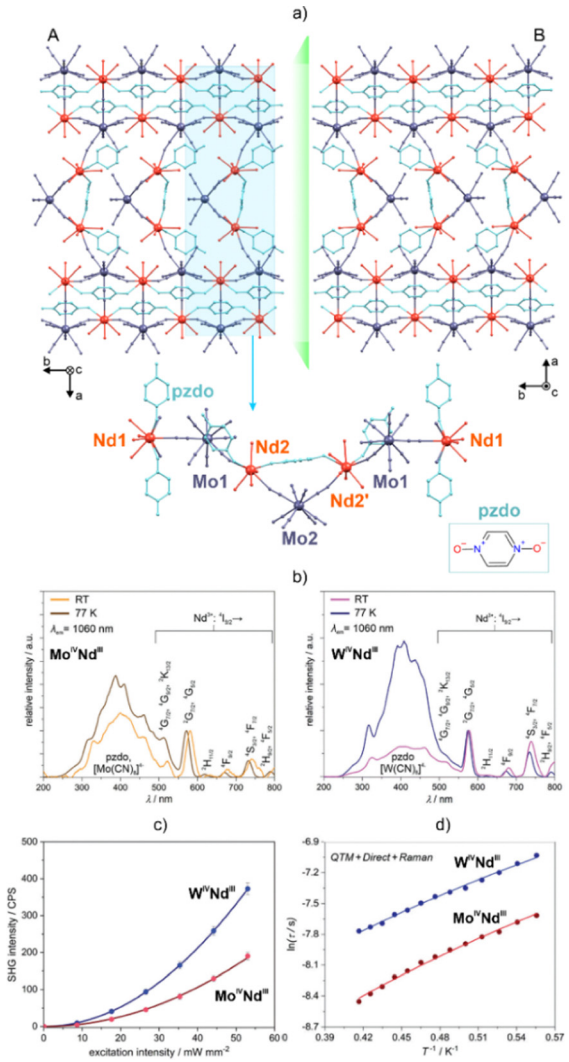

Fig. 18 (a) Structural view of the $\{[Nd^{III}_4(H_2O)_{17}(pzdo)_5][M^{IV}(CN)_8]_3\}\cdot 9H_2O$ coordination polymers (M = Mo ($Mo^{IV}Nd^{III}$), W ($W^{IV}Nd^{III}$); pzdo = pyrazine *N,N′*-dioxide),[308] (b) their excitation spectra for the 1060 nm emission, (c) their SHG signals at 300 K, and (d) temperature dependence of the magnetic relaxation times. Parts (b–d) were reproduced from ref. 308 with permission from the Royal Society of Chemistry.

cyanidometallates, these compounds crystallize in the non-centrosymmetric *C*2 space group as a mixture of two enantiomorphs, A and B. Owing to these features, they exhibit SHG activity that coexists with the sensitized Nd(III)-centred photoluminescence and the slow magnetic relaxation effect. Furthermore, they exemplify the modulating role of octacyanidometallates in the tuning of each of the listed functionalities. Firstly, the substitution of a d-block metal increases the sensitization efficiency at low temperatures. At room temperature, for both the Nd–W and Nd–Mo compounds, the UV-to-visible excitation band, which is related to the energy transfer route, stays at a similar level as the direct f–f excitation band, suggesting the comparable efficiency of both types of excitation pathway. By contrast, at low temperatures, the energy transfer route starts to dominate over the direct f–f excitation pathway, due to the limitation of the deactivation processes. The W(IV)-based analogue is characterized by a much stronger temperature dependence, being a better sensitizer at the low-temperature regime, which is presumably related to the fact that donor states of the $[W^{IV}(CN)_8]^{4-}$ moieties are situated closer to the acceptor states of the Nd(III) centres. Secondly, the Mo-to-W replacement enhances the SH intensity which can be explained by the modulation of an ionic radius, resulting in a change in the polarizability. Finally, the $[M^{IV}(CN)_8]^{4-}$ anion exchange affects the SMM behaviour, which is related to the subtle but non-negligible structural variation around the Nd^{III} centre.

5.2 Circularly polarized luminescence in chiral luminescent lanthanide SMMs

Research concerning CPL-active materials is fuelled by attractive applications in display technologies, including the construction of CP-LEDs. Moreover, circularly polarized light can be utilized in the field of optical information storage, optical sensors, and optical communication.[304–306] The large efforts in this research field are related to the design of luminophores that provide a large dissymmetry factor, g_{lum}, and Ln(III) complexes are promising candidates in this context.[309,310] Therefore, the Ln-SMMs are worth studying for their CPL activity, which was very recently initiated by a few research groups.[311–313] The additional promising perspective for the exploration of CPL in Ln(III)-based molecular nanomagnets is related to the great sensitivity of this optical phenomenon to external stimuli.[304,314,315] As a result, a strong influence of the SMM properties, *e.g.*, magnetic memory effect, on the CPL signal is expected; thus, it can be considered as a potential optical output for related magnetic data storage devices. Among the pioneering studies on chiral Ln-SMMs that show circularly polarized luminescence, the pair of enantiomers reported by Sutter *et al.*, *i.e.*, $[L^{Me2}Zn^{II}(Cl)Dy^{III}((\pm)camph)_2\ (MeOH)]$ (*Λ*-Dy and *Δ*-Dy) (ligands presented in Fig. 19), deserve special attention (Fig. 19).[311] The authors demonstrated the concomitant emergence of the CPL and SMM effect in the solid state for an enantiomeric pair of these chiral Dy^{III} complexes. It is worth mentioning that the recognized CPL was found to be significant, reaching the g_{lum} value of +0.18 for *Λ*-Dy. The identical CPL effect was found for either a single-crystalline material or a polycrystalline powder, which constitutes another important outcome of this work, suggesting that the CPL effect is not restricted to a single crystal. It is also essential to mention that the g_{lum} increase is inversely proportional to the temperature, and above 25 K the emission almost disappears. Moreover, the increase in the g_{lum} value in the low-temperature regime corresponds to the occurrence of slow relaxation of magnetization. Taking into consideration that CPL can be generated not only by the chirality of a given structure but also by a magnetic field, isostructural Eu(III)-based analogues have been investigated to estimate the contribution of both factors. Interestingly, for the Eu(III) counterparts, down to 5 K, the emission is identical for the two circular polarizations. Furthermore, the g_{lum} factor value was found to be close to 0, excluding a crucial role of the structural factor in the observed effect and indicating the pivotal role of magnetization blocking in the CPL phenomenon.

Recently, another example of the CPL-active SMM was reported by Pointillart and co-workers (Fig. 20).[313] They demonstrated new results concerning the previously reported chiral

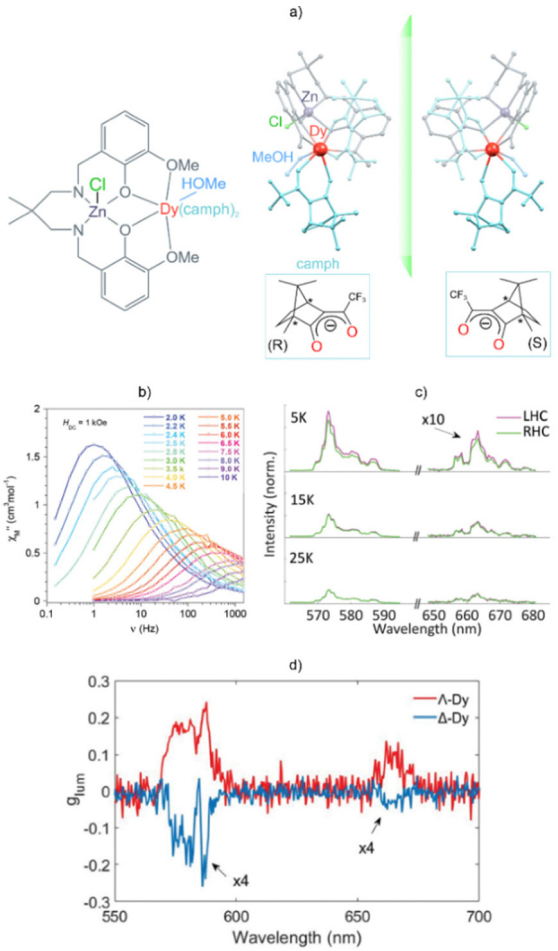

Fig. 19 (a) Structural view of the chiral [$L^{Me2}Zn^{II}(Cl)Dy^{III}((\pm)camph)_2$-(MeOH)] molecules ($\Lambda$-Dy and Δ-Dy enantiomers),[311] (b) representative ac magnetic characteristics under a dc field of 1000 Oe for Λ-Dy diluted with Y(III), (c) temperature-dependent emission spectra for Λ-Dy (where LHC and RHC correspond to the left- and right-handed circular polarizations, respectively), and (d) CPL spectra at T = 5 K for Λ-Dy and Δ-Dy. Parts (b–d) were adapted from ref. 311 with permission from the Royal Society of Chemistry.

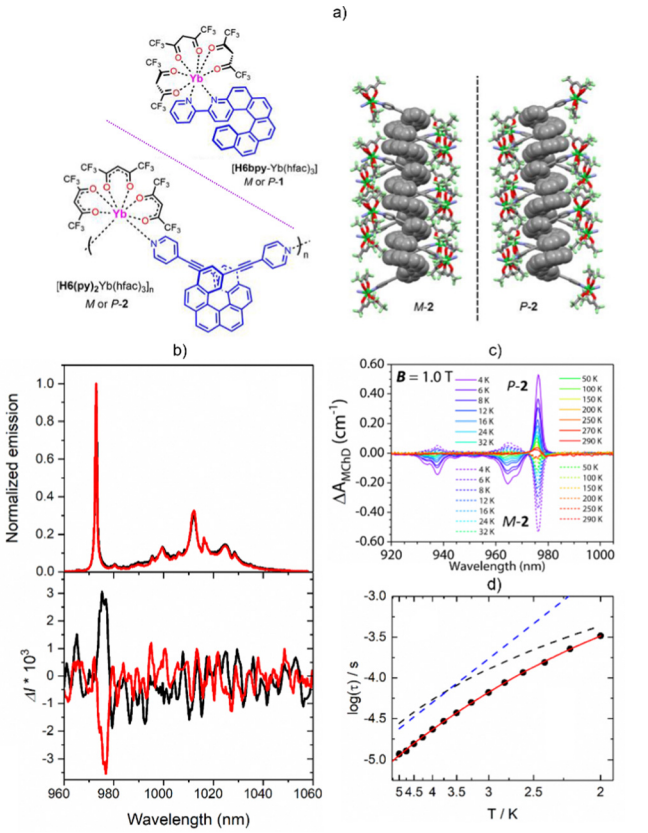

Fig. 20 (a) Schematic representation of the structures of the [H6bpy-$Yb^{III}(hfac)_3$] (M/P-1) and [$H6(py)_2Yb^{III}(hfac)_3]_n$ (M/P-2) coordination systems together with the supramolecular arrangement of the M/P-2 enantiomers along the *a* axis,[313] (b) total luminescence recorded at 77 K (top) and the related CPL spectra measured at 298 K under 365 nm excitation (bottom) for M/P-2 (where the spectra for the *P* and *M* enantiomers are depicted in red and black, respectively), and the (c) temperature and (d) magnetic field dependence of the MChD spectra for *P*-2 and *M*-2. Adapted with permission from ref. 313. Copyright 2015 John Wiley & Sons.

molecules[133] [H6bpy-$Yb^{III}(hfac)_3$] (M/P-1; hfac = 1,1,1,5,5,5-hexafluoroacetylacetonate; the H6bpy ligand is shown in Fig. 20), and the unique chiral coordination chains [$H6(py)_2$-$Yb^{III}(hfac)_3]_n$ (M/P-2), based on the Yb(III) centres bearing helicene-type ligands, that exhibit a NIR-range CPL signal and the slow magnetic relaxation effect. In the second compound, the helicene ligands connected with the [$Yb^{III}(hfac)_3$] moieties led to the assembly of a polymeric structure characterized by the presence of ligand-based columns, providing the first example of helicene-based Ln(III)-containing coordination chains. Reliable mirror-imaged CPL spectra were recorded for both materials. For *M*-1, two CPL-active bands can be observed with g_{lum} values of −0.13, and +0.02, whereas the band characterized by g_{lum} = +0.007 was recognized for *M*-2. The better CPL performance for M/P-1 was rationalized by the stronger dissymmetric environment of the Yb^{3+} ions. Moreover, in the case of M/P-1 and M/P-2, the intertwining of chirality and magnetism led to the emergence of the MChD response. Considering M/P-2, three main MChD signals are observed for each enantiomer, which can be ascribed to the $^2F_{7/2} \rightarrow {}^2F_{5/2}$ electronic transitions of the Yb^{3+} ion. The intensity of the MChD signals at 976 nm, which are related to the $0 \rightarrow 0'$ line, turned out to be high, reaching a value close to about 0.50 cm^{-1} at 1 T. The MChD effect in comparison with the overall absorption, expressed by a g_{MChD} factor equal to 0.19 T^{-1}, is one of the highest reported for Ln(III) complexes. This value is one and a half times higher than that postulated for the M/P-1 pair. The MChD enhancement in M/P-2 was ascribed to the differences in the coordination sphere and/or magnetic anisotropy for the Ln(III) centres in both types of compound. The comparative analysis led to the important conclusion that, in generating the strong MChD effect, magnetic anisotropy can be considered a more dominant factor than the chirality of the Ln(III) complex.

6. Conclusions and perspectives

Complexes of trivalent Ln ions were found to be efficient molecular building blocks for the construction of luminescent

molecular nanomagnets since their designable coordination sphere can ensure both strong tunable luminescence and significant magnetic anisotropy, giving single-molecule magnet (SMM) behaviour. The research of the past few years summarized in this feature article shows that luminescent Ln-based SMMs can be further functionalized towards advanced multifunctional materials. In this regard, three main research pathways were formulated.

The first concerns the exploration of emissive Ln-SMMs as stimuli-responsive systems in which both the optical and magnetic features are modulated using a chemical or physical stimulus. It was presented that the reversible desolvation of the crystal lattice containing the Ln complexes can be used to switch or even generate the luminescent molecular nanomagnets. In an analogous way, light irradiation was presented to efficiently modulate the magneto-luminescence properties of Ln(III) complexes, opening a route to unique photo-switches. The luminescent Ln-SMMs were also employed as optical thermometers due to the sensitivity of the emission pattern to variations in the temperature. Various approaches, including the exploration of hot emission bands, the re-absorption effect or Raman spectroscopy, were used to achieve a high-performance thermometric effect. It can be even realized in a temperature range close to the operating regime of SMMs, and thus such a magnetic system can uniquely self-monitor its temperature.

The second type of the functionalization of emissive Ln-SMMs is related to the generation of electrical functionalities, ranging from ionic and electronic conductivity to pyro-, piezo- and ferroelectricity. The enriched multifunctionality was achieved when negatively charged emissive Ln-SMMs were combined with acidic cations, resulting in a proton-conductive luminescent thermometer based on a NIR-emissive molecular nanomagnet. For this material, the remarkable co-existence of a few physical functionalities in the single-phase material was presented, but even more impressive results were found when ferroelectricity was introduced into the Ln-SMM-based framework. For such a material, a strong magneto-electric coupling, realized through magnetic control over the electric polarization, was reported.

The third strategy towards multifunctional systems based on Ln-SMMs consists of the implementation of 4f metal complexes into non-centrosymmetric and/or chiral structures, which opens perspectives for optical effects such as MChD, SHG, and CPL. These physical phenomena were generated for unique solids based on luminescent Ln-SMMs; however, their strong coupling with the SMM properties has not yet been fully recognized due to the low values of the magnetic blocking temperatures. Nevertheless, one can notice that luminescent Ln-based SMMs have proved to be a great starting point for multifunctional materials. The stronger correlation, particularly between the SMM properties which include the magnetic memory effect, and the other introduced properties, is a future challenge. It will demand advances in the instrumentation as well as better strategies for the enhancement of magnetic anisotropy, enabling the broad temperature overlap of the operating ranges of magnetic, luminescent, and added physical effects.

Within our contribution to this research field, we proved that the heterometallic approach, which uses the functionalization of Ln(III) complexes by cyanido-based metalloligands with the support of organic ligands, is one of the most efficient routes for incorporating various effects, including the sensitivity to humidity and solvent exchange, optical thermometry of diverse mechanisms, high proton conductivity, and the SHG activity. Taking into account the versatile character of cyanido metal complexes which can be variously modified and supported using non-innocent organic ligands and counter-ions, it is expected that other possible physical functionalities, such as ferroelectricity or CPL, are accessible within the approach explored by us, and this will be tested soon. Among other perspectives, it is worth mentioning that the great undiscovered potential concerns the exploration of uncommon Ln ions. This includes Ce(III) centres which exhibit emission related to d–f electronic transitions that is expected to be more sensitive to external stimuli than the emission originating from f–f electronic transitions. Moreover, divalent Ln ions remain unexplored as a source of luminescent SMMs and related subsequent multifunctional systems, despite the expected remarkable optical and magnetic properties.[170] Another underexplored field is related to the different sides of Ln emission, including the use of up-conversion luminescence or the use of electroluminescence. The broadening of the spectrum of external stimuli used for switching of the properties of emissive Ln-SMMs towards, for example, pressure or mechanical action, is also worth considering. Last but not least, a future challenge consists of the conjunction of a few strategies to achieve next-level multifunctionality, *e.g.*, chemical or photoswitching effects on the electrical or chirality-related optical phenomena in emissive Ln-SMMs. It is expected that breakthroughs along these lines will soon emerge.

Conflicts of interest

There are no conflicts to declare.

Acknowledgements

This work was funded by the European Union (ERC, LUMIFIELD, 101042112). Views and opinions expressed are, however, those of the authors only and do not necessarily reflect those of the European Union or the European Research Council. Neither the European Union nor the granting authority can be held responsible for them. The work related to the combination of electrical and luminescent properties (Section 4) was financed by the National Science Centre, Poland, within the SONATA BIS-9 project, grant no. 2019/34/E/ST5/00148. The open-access publication of this article has been supported by a grant from the Faculty of Chemistry under the Strategic Programme Excellence Initiative at Jagiellonian University.

References

1 M. Ko, L. Mendecki and K. A. Mirica, *Chem. Commun.*, 2018, **54**, 7873–7891.

2 H. Kim, S. Beack, S. Han, M. Shin, T. Lee, Y. Park, K. S. Kim, A. K. Yetisen, S. H. Yun, W. Kwon and S. K. Hahn, *Adv. Mater.*, 2018, **30**, 1701460.
3 G.-H. Lee, H. Moon, H. Kim, G. H. Lee, W. Kwon, S. Yoo, D. Myung, S. H. Yun, Z. Bao and S. K. Hahn, *Nat. Rev. Mater.*, 2020, **5**, 149–165.
4 Z. Wang and W. Qin, *NPG Asia Mater.*, 2021, **13**, 17(12).
5 W. Zhang and M. Yashima, *Chem. Commun.*, 2023, **59**, 134–152.
6 G. Long, R. Sabatini, M. I. Saidaminov, G. Lakhwani, A. Rasmita, X. Liu, E. H. Sargent and W. Gao, *Nat. Rev. Mater.*, 2020, **5**, 423–439.
7 L. Kang and Z. Lin, *Light Sci. Appl.*, 2022, **11**, 201(12).
8 X. Zheng, R. K. Kankala, C.-G. Liu, Y. Wen, S.-B. Wang, A.-Z. Chen and Y. Zhang, *Adv. Optical Mater.*, 2022, **10**, 2200167(15).
9 Z. Jiang, P. Wang, J. Xing, X. Jiang and J. Zhao, *ACS Appl. Mater. Interfaces*, 2018, **10**, 39032–39039.
10 G. C. Thaggard, J. Haimerl, K. C. Park, J. Lim, R. A. Fischer, B. K. P. M. Kankanamalage, B. J. Yarbrough, G. R. Wilson and N. B. Shustova, *J. Am. Chem. Soc.*, 2022, **144**, 2324–23263.
11 A. Dsouza, C. Constantinidou, T. N. Arvanitis, D. M. Haddleton, J. Charment and R. A. Hand, *ACS Appl. Mater. Interfaces*, 2022, **14**, 47323–47344.
12 Y. Li, J. Tang, L. he, Y. Liu, C. Chen and Z. Tang, *Adv. Mater.*, 2015, **27**, 4070–4080.
13 T. Wehner, M. T. Seuffert, J. R. Sorg, M. Schneider, K. Mandel, G. Sextl and K. Müller-Buschbaum, *J. Mater. Chem. C*, 2017, **5**, 10133–10142.
14 J. Hao, Y. Zhang and X. Wei, *Angew. Chem., Int. Ed.*, 2011, **123**, 7008–7012.
15 V. Rubio-Gimenez, S. Tatay and C. Marti-Gastaldo, *Chem. Soc. Rev.*, 2020, **49**, 5601–5638.
16 Z. Meng and K. A. Mirica, *Chem. Soc. Rev.*, 2021, **50**, 13498–13558.
17 S. Ohkoshi, S. Takano, K. Imoto, M. Yoshikiyo, A. Namai and H. Tokoro, *Nat. Photonics*, 2014, **8**, 65–71.
18 C. Lochenie, K. Schötz, F. Panzer, H. Kurz, B. Maier, F. Puchtler, S. Agarwal, A. Köhler and B. Weber, *J. Am. Chem. Soc.*, 2018, **140**, 700–709.
19 S. Garg, H. Schwartz, M. Kozlowska, A. B. Kanj, M. Müller, W. Wenzel, U. Ruschewitz and L. Heinke, *Angew. Chem., Int. Ed.*, 2019, **58**, 1193–1197.
20 X. Wang, C.-N. Xu, H. Yamada, K. Nishikubo and X.-G. Zheng, *Adv. Mater.*, 2005, **17**, 1254–1258.
21 T. Nuida, T. Matsuda, H. Tokoro, S. Sakurai, K. Hashimoto and S. Ohkoshi, *J. Am. Chem. Soc.*, 2005, **127**, 11604–11605.
22 Y. Kitagawa, Y. Hiraoka, T. Honda, T. Ishikura, H. Nakamura and T. Kimura, *Nat. Mater.*, 2010, **9**, 797–802.
23 Z. Zhang, P.-F. Li, Y.-Y. Tanh, A. J. Wilson, K. Willets, M. Wuttig, R.-G. Xiong and S. Ren, *Sci. Adv.*, 2017, **3**, e1701008(7).
24 B. Owens-Baird, J. Xu, D. Y. Petrovykh, O. Bondarchuk, Y. Ziouani, N. Gonzalez-Ballesteros, P. Yox, F. M. Sapountzi, H. Niemants-verdriet, Y. V. Kolen'ko and K. Kovnir, *Chem. Mater.*, 2019, **31**, 3407–3418.
25 C. Shu, N. Zhang, Y. Gao, J. An, X. Wen, W. Ma, Z. Liu, B. Sun and S. Li, *ACS Appl. Mater. Interfaces*, 2022, **14**, 24648–24658.
26 W. Li, Z. Wang, F. Deschler, S. Gao, R. H. Friend and A. K. Cheetham, *Nat. Rev. Mater.*, 2017, **2**, 16099.
27 A. Kirchon, L. Feng, H. F. Drake, E. A. Joseph and H.-C. Zhou, *Chem. Soc. Rev.*, 2018, **47**, 8611–8638.
28 L. Kortekaas and W. R. Browne, *Chem. Soc. Rev.*, 2019, **48**, 3406–3424.
29 G. Li, D. Zhu, X. Wang, Z. Su and M. R. Bryce, *Chem. Soc. Rev.*, 2020, **49**, 765–838.
30 P. Sarkar, I. H. Chowdury, S. Das and S. M. Islam, *Mater. Adv.*, 2022, **3**, 8063–8080.
31 J. M. Cameron, G. Guillemot, T. Galambos, S. S. Amin, E. Hampson, K. M. Haidaraly, G. N. Newton and G. Izzet, *Chem. Soc. Rev.*, 2022, **51**, 293–328.
32 Y. Zhang, W.-Q. Liao, D.-W. Fu, H.-Y. Ye, Z.-N. Chen and R.-G. Xiong, *J. Am. Chem. Soc.*, 2015, **137**, 4928–4931.
33 Y. Wu, H. Jiang, S. Jiao, D. Li, Z. Gao, B. Niu, D. Wu, S. Chen, H.-L. Cai and X. Wu, *Adv. Optical Mater.*, 2022, **10**, 2101905(8).
34 C. Train, T. Nuida, R. Gheorghe, M. Gruselle and S. Ohkoshi, *J. Am. Chem. Soc.*, 2009, **131**, 16838–16843.
35 T. Ohno, K. Nakabayashi, K. Imoto, M. Komine, S. Chorazy and S. Ohkoshi, *CrystEngComm*, 2018, **20**, 7236–7241.
36 E. Pardo, C. Train, H. Liu, L.-M. Chamoreau, B. Dkhil, K. Boubekeur, F. Lloret, K. Nakatani, H. Tokoro, S. Ohkoshi and M. Verdaguer, *Angew. Chem., Int. Ed.*, 2012, **51**, 8356–8360.
37 L. C. Gomez-Aguirre, B. Pato-Doldan, J. Mira, S. Castro-Garcia, M. A. Senaris-Rodriguez, M. Sanchez-Andujar, J. Singleton and V. S. Zapf, *J. Am. Chem. Soc.*, 2016, **138**, 1122–1125.
38 K. Müller, J. Wadhwa, J. S. Malhi, L. Schöttner, A. Welle, H. Schwartz, D. Hermann, U. Ruschewitz and L. Heinke, *Chem. Commun.*, 2017, **53**, 8070–8073.
39 S. Ohkoshi, K. Nakagawa, K. Imoto, H. Tokoro, Y. Shibata, K. Okamoto, Y. Miyamoto, M. Komine, M. Yoshikiyo and A. Namai, *Nat. Chem.*, 2020, **12**, 338–344.
40 G. Azzolina, H. Tokoro, K. Imoto, M. Yoshikiyo, S. Ohkoshi and E. Collet, *Angew. Chem., Int. Ed.*, 2021, **60**, 23267–23273.
41 K. Günther, N. Grabicki, B. Battistella, L. Grubert and O. Dumele, *J. Am. Chem. Soc.*, 2022, **144**, 8707–8716.
42 A. Watanabe, A. Kobayashi, E. Saitoh, Y. Nagao, M. Yoshida and M. Kato, *Inorg. Chem.*, 2015, **54**, 11058–11060.
43 S. Chorazy, R. Podgajny, W. Nogaś, S. Buda, W. Nitek, J. Mlynarski, M. Rams, M. Kozieł, E. Juszyńska Gałązka, V. Vieru, L. F. Chibotaru and B. Sieklucka, *Inorg. Chem.*, 2015, **54**, 5784–5794.
44 D. Chen, H. Xing, Z. Su and C. Wang, *Chem. Commun.*, 2016, **52**, 2019–2022.
45 K. Kon, K. Uchida, K. Fuku, S. Yamanaka, B. Wu, D. Yamazui, H. Iguchi, H. Kobayashi, Y. Gambe, I. Honma and S. Takaishi, *ACS Appl. Mater. Interfaces*, 2021, **13**, 38188–38193.
46 J. Perego, C. X. Bezuidenhout, I. Villa, F. Cova, R. Crapanzano, I. Frank, F. Pagano, N. Kratochwill, E. Auffray, S. Bracco, A. Vedda, C. Dujardin, P. E. Sozzani, F. Meinardi, A. Comotti and A. Monguzzi, *Nat. Commun.*, 2022, **13**, 3054(10).
47 J. Rocha, L. D. Carlos, F. A. Almeida Paz and D. Ananias, *Chem. Soc. Rev.*, 2011, **40**, 926–940.
48 Y. Zhang, S. Liu, Z.-S. Zhao, Z. Wang, R. Zhang, L. Liu and Z.-B. Han, *Inorg. Chem. Front.*, 2021, **8**, 590–619.
49 E. Echenique-Errandonea, R. F. Mendes, F. Figueira, D. Choquesillo-Lazarte, G. Beobide, J. Cepeda, D. Ananias, A. Rodriguez-Dieguez, F. A. Almeida Paz and J. M. Seco, *Inorg. Chem.*, 2022, **61**, 12977–12990.
50 S. V. Eliseeva and J.-C. G. Bünzli, *Chem. Soc. Rev.*, 2010, **39**, 189–227.
51 G. Bao, K.-L. Wong, D. Jin and P. A. Tanner, *Light Sci. Appl.*, 2018, **7**, 96(10).
52 M. Suta, N. Harmgarth, M. Kühling, P. Liebing, F. T. Edelmann and C. Wickleder, *Chem. Asian J.*, 2018, **13**, 1038–1044.
53 J.-C. G. Bünzli, *Coord. Chem. Rev.*, 2015, **293–294**, 19–47.
54 Y. Hasegawa, Y. Kitagawa and T. Nakanishi, *NPG Asia Mater.*, 2018, **10**, 52–70.
55 M. S. Khan, R. Ilmi, W. Sun, J. D. L. Dutra, W. F. Oliviera, L. Zhou, W.-Y. Wong and P. R. Raithby, *J. Mater. Chem. C*, 2020, **8**, 5600–5612.
56 H. Yao, G. Calvez, C. Daiguebonne, Y. Suffren, K. Bernot, T. Roisnel and O. Guillou, *Inorg. Chem.*, 2022, **61**, 4895–4908.
57 S. SeethaLekhsmi, A. R. Ramya, M. L. P. Reddy and S. Varughese, *J. Photochem. Photobiol. C: Photochem. Rev.*, 2017, **33**, 109–131.
58 T. N. Nguyen, S. V. Eliseeva, A. Gładysiak, S. Petoud and K. C. Stylianou, *J. Mater. Chem. A*, 2020, **8**, 10188–10192.
59 B. Golesorkhi, S. Naseri, L. Guenee, I. Taarit, F. Alves, H. Nozary and C. Piguet, *J. Am. Chem. Soc.*, 2021, **143**, 15326–15334.
60 Y. Xie, G. Sun, G. A. Mandl, S. L. Maurizio, J. Chen, J. A. Capobianco and L. Sun, *Angew. Chem., Int. Ed.*, 2023, e202216269(7).
61 F. Zinna, U. Giovanella and L. Di Bari, *Adv. Mater.*, 2015, **27**, 1791–1795.
62 Y. Ou, W. Zhou, Z. Zhu, F. Ma, R. Zhou, F. Su, L. Zheng, L. Ma and H. Liang, *Angew. Chem., Int. Ed.*, 2020, **59**, 23810–23816.
63 A. M. Kaczmarek, Y.-Y. Liu, C. Wang, B. Laforce, L. Vincze, P. Van Der Voort, K. Van Hecke and R. Van Deun, *Adv. Funct. Mater.*, 2017, **27**, 1700258(5).
64 D. F. Sava Gallis, L. E. S. Rohwer, M. A. Rodriguez, M. C. Barnhart-Dailey, K. S. Butler, T. S. Luk, J. A. Timlin and K. W. Chapman, *ACS Appl. Mater. Interfaces*, 2017, **9**, 22268–22277.
65 F. G. Moscoso, J. Almeida, A. Sousaraei, T. Lopes-Costa, A. M. G. Silva, J. Cabanillas-Gonzalez, L. Cunha-Silva and J. M. Pedrosa, *J. Mater. Chem. C*, 2020, **8**, 3626–3630.
66 L. Wang and Y. Chen, *Chem. Commun.*, 2020, **56**, 6965–6968.
67 G. E. Gomez, R. Marin, A. N. Carneiro Neto, A. M. P. Botas, J. Ovens, A. A. Kitos, M. C. Bernini, L. D. Carlos, J. A. A. Soler-Illia and M. Murugesu, *Chem. Mater.*, 2020, **32**, 7458–7468.

68 V. Trannoy, A. N. Carneiro Neto, C. D. S. Brites, L. D. Carlos and H. Serier-Brault, *Adv. Optical Mater.*, 2021, **9**, 2001938(12).
69 S. T. Liddle and J. van Slageren, *Chem. Soc. Rev.*, 2015, **44**, 6655–6669.
70 Z. Zhu and J. Tang, *Nat. Sci. Rev*, 2022, **9**, 12.
71 Z. Zhu and J. Tang, *Chem. Soc. Rev.*, 2022, **51**, 9469–9481.
72 J. Liu, Y.-C. Chen, J.-L. Liu, V. Vieru, L. Ungur, J.-H. Jia, L. F. Chibotaru, Y. Lan, W. Wernsdorfer, S. Gao, X.-M. Chen and M.-L. Tong, *J. Am. Chem. Soc.*, 2016, **138**, 5441–5450.
73 F.-S. Guo, B. M. Day, Y.-C. Chen, M.-L. Tong, A. Mansikkamäki and R. A. Layfield, *Science*, 2018, **362**, 1400–1403.
74 A. B. Canaj, S. Dey, E. Regincos Marti, C. Wilson, G. Rajaraman and M. Murrie, *Angew. Chem., Int. Ed.*, 2019, **58**, 14146–14151.
75 T. P. Latandresse, V. Vieru, B. O. Wilkins, N. S. Bhunavanesh, L. F. Chibotaru and M. Nippe, *Angew. Chem., Int. Ed.*, 2018, **57**, 8164–8169.
76 C. A. Gould, K. R. McClain, D. Reta, J. G. C. Kragskow, D. A. Marchion, E. Lachman, E.-S. Choi, J. G. Analytis, R. D. Britt, N. F. Chilton, B. G. Harvey and J. R. Long, *Science*, 2022, **375**, 198–202.
77 J. J. LeRoy, L. Ungur, I. Korobkov, L. F. Chibotaru and M. Murugesu, *J. Am. Chem. Soc.*, 2014, **136**, 8003–8010.
78 A. J. Brown, D. Pinkowicz, M. R. Saber and K. R. Dunbar, *Angew. Chem., Int. Ed.*, 2015, **54**, 5864–5868.
79 C. Wäckerlin, F. Donati, A. Singha, R. Baltic, S. Rusponi, K. Diller, F. Patthey, M. Pivetta, Y. Lan, S. Klyatskaya, M. Ruben, H. Brune and J. Dreiser, *Adv. Mater.*, 2016, **28**, 5195–5199.
80 L. Spree, F. Liu, V. Neu, M. Rosenkranz, G. Velkos, Y. Wang, S. Schiemenz, J. Dreiser, P. Gargiani, M. Valvidares, C.-H. Chen, B. Büchner, S. M. Avdoshenko and A. A. Popov, *Adv. Funct. Mater.*, 2021, **31**, 2105516(7).
81 G. Cucinotta, M. Perfetti, J. Luzon, M. Etienne, P.-E. Car, A. Caneschi, G. Calvez, K. Bernot and R. Sessoli, *Angew. Chem., Int. Ed.*, 2012, **51**, 1606–1610.
82 J. Long, Y. Guari, R. A. S. Ferreira, L. D. Carlos and J. Larionova, *Coord. Chem. Rev.*, 2018, **363**, 57–70.
83 R. Marin, G. Brunet and M. Murugesu, *Angew. Chem., Int. Ed.*, 2021, **60**, 1728–1746.
84 C. C. Beedle, C. J. Stephenson, K. J. Heroux, W. Wernsdorfer and D. N. Hendrickson, *Inorg. Chem.*, 2008, **47**, 10798–10800.
85 K. Kumar, G. Li, O. Stefanczyk, S. Chorazy, K. Nakabayashi and S. Ohkoshi, *J. Mater. Chem. C*, 2023, **11**, 1008–1020.
86 C. A. Mattei, V. Montigaud, V. Dorcet, F. Riobe, G. Argouarch, O. Maury, B. Le Guennic, O. Cador, C. Lalli and F. Pointillart, *Inorg. Chem. Front.*, 2021, **8**, 963–976.
87 S. Shintoya, K. Murakami, T. Fujinami, N. Matsumoto, N. Mochida, T. Ishida, Y. Sunatsuki, M. Watanabe, M. Tsuchimoto, J. Mrozinski, C. Coletti and N. Re, *Inorg. Chem.*, 2014, **53**, 10359–10369.
88 S. Chorazy, T. Charytanowicz, J. Wang, S. Ohkoshi and B. Sieklucka, *Dalton Trans.*, 2018, **47**, 7870–7874.
89 M. Nie, J. Xiong, C. Zhao, H. Meng, K. Zhang, Y. Han, J. Li, B. Wang, L. Feng, C. Wang and T. Wang, *Nano Res.*, 2019, **12**, 1727–1731.
90 F. Pointillart, B. Le Guennic, S. Golhen, O. Cador, O. Maury and L. Ouahab, *Chem. Commun.*, 2013, **49**, 615–617.
91 Y.-C. Chen, J.-L. Liu, Y. Lan, Z.-Q. Zhong, A. Mansikkamäki, L. Ungur, Q.-W. Li, J.-H. Jia, L. F. Chibotaru, J.-B. Han, W. Wernsdorfer, X.-M. Chen and M.-L. Tong, *Chem. – Eur. J.*, 2017, **23**, 5708–5715.
92 Y. Bi, C. Chen, Y.-F. Zhao, Y.-Q. Zhang, S.-D. Jiang, B.-W. Wang, J.-B. Han, J.-L. Sun, Z.-Q. Bian, Z.-M. Wang and S. Gao, *Chem. Sci.*, 2016, **7**, 5020–5031.
93 J. D. Rinehart and J. R. Long, *Chem. Sci.*, 2011, **2**, 2078–2085.
94 J.-C. G. Bünzli and C. Piguet, *Chem. Soc. Rev.*, 2005, **34**, 1048–1077.
95 X. Liu, C. Zhao, J. Wu, Z. Zhu and J. Tang, *Dalton Trans.*, 2022, **51**, 16444–16447.
96 Z. Zhu, C. Zhao, Q. Zhou, S. Liu, X.-L. Li, A. Mansikkamäki and J. Tang, *CCS Chem.*, 2022, **4**, 3762–3771.
97 Z. Zhu, G.-Q. Jin, J. Wu, X. Ying, C. Zhao, J.-L. Zhang and J. Tang, *Inorg. Chem. Front.*, 2022, **9**, 5048–5054.
98 S. Liu, Y. Gil, C. Zhao, J. Wu, Z. Zhu, X.-L. Li, D. Aravena and J. Tang, *Inorg. Chem. Front.*, 2022, **9**, 4982–4989.
99 J. Wu, G.-L. Wang, Z. Zhu, C. Zhao, X.-L. Li, Y.-Q. Zhang and J. Tang, *Chem. Commun.*, 2022, **58**, 7638–7641.
100 K. Fan, S.-S. Bao, R. Huo, X.-D. Huang, Y.-J. Liu, Z.-W. Yu, M. Kurmoo and L.-M. Zheng, *Inorg. Chem. Front.*, 2020, **7**, 4580–4592.
101 S. Chorazy, M. Rams, K. Nakabayashi, B. Sieklucka and S. Ohkoshi, *Chem. – Eur. J.*, 2016, **22**, 7371–7375.
102 M. Liberka, M. Zychowicz, W. Zychowicz and S. Chorazy, *Chem. Commun.*, 2022, **58**, 6381–6384.
103 N. Hoshino, F. Iijima, G. N. Newton, N. Yoshida, T. Shiga, H. Nojiri, A. Nakao, R. Kumai, Y. Murakami and H. Oshio, *Nat. Chem.*, 2012, **4**, 921–926.
104 E. S. Koumousi, I.-R. Jeon, Q. Gao, P. Dechambenoit, D. N. Woodruff, P. Merzeau, L. Buisson, X. Jia, D. Li, F. Volatron, C. Mathoniere and R. Clerac, *J. Am. Chem. Soc.*, 2014, **136**, 15461–15464.
105 S. Chorazy, K. Nakabayashi, S. Ohkoshi and B. Sieklucka, *Chem. Mater.*, 2014, **26**, 4072–4075.
106 M. Atzori, I. Breslavetz, K. Paillot, K. Inoue, G. L. J. A. Rikken and C. Train, *J. Am. Chem. Soc.*, 2019, **141**, 20022–20025.
107 S. Chorazy, J. J. Zakrzewski, M. Magott, T. Korzeniak, B. Nowicka, D. Pinkowicz, R. Podgajny and B. Sieklucka, *Chem. Soc. Rev.*, 2020, **49**, 5945–6001.
108 J. J. Zakrzewski, M. Liberka, M. Zychowicz and S. Chorazy, *Inorg. Chem. Front.*, 2021, **8**, 452–483.
109 R. Turo-Cortes, M. Meneses-Sanchez, T. Delgado, C. Bartual-Murgui, M. Carmen Munoz and J. A. Real, *J. Mater. Chem. C*, 2022, **10**, 10686–10698.
110 S. Dang, J.-H. Zhang, Z.-M. Sun and H. Zhang, *Chem. Commun.*, 2012, **48**, 11139–11141.
111 Y.-Q. Sun, Q. Liu, L.-H. Liu, L. Ding and Y.-P. Chen, *New J. Chem.*, 2017, **41**, 6736–6741.
112 Y. Wang, J. Wang, H. Shu, B. Cheng, Z. He, P. Wang and T. Xia, *Inorg. Chem.*, 2021, **60**, 7345–7350.
113 A. Kobayashi, S. Imada, Y. Shigeta, Y. Nagao, M. Yoshida and M. Kato, *J. Mater. Chem. C*, 2019, **7**, 14923–14931.
114 Y. Zorlu, L. Wagner, P. Tholen, M. M. Ayhan, C. Bayraktar, G. Hanna, A. O. Yazaydin, Ö. Yavuzcetin and G. Yücesan, *Adv. Optical Mater.*, 2022, **10**, 2200213(7).
115 P. Wu, J. Wang, Y. Li, C. He, Z. Xie and C. Duan, *Adv. Funct. Mater.*, 2011, **21**, 2788–2794.
116 P. Wu, L. Xia, M. Huangfu, F. Fu, M. Wang, B. Wen, Z. Yang and J. Wang, *Inorg. Chem.*, 2020, **59**, 264–273.
117 J.-P. Bai, Y.-L. Huang, M. Xie, Y. Zhao, D. Luo, Y. Y. Li, W. Lu and D. Li, *ACS Appl. Mater. Interfaces*, 2019, **11**, 38503–38509.
118 P. Majee, P. Daga, D. K. Singha, D. Saha, P. Mahata and S. K. Mondal, *J. Photochem. Photobiol. A: Chem.*, 2020, **402**, 112830.
119 P. Zhang, N. Song, S. Liu, Q. Li, Y. Wang and B. Zhou, *J. Mater. Chem. C*, 2021, **9**, 6208–6216.
120 T. Xia, Y. Wan, Y. Li and J. Zhang, *Inorg. Chem.*, 2020, **59**, 8809–8817.
121 X. Liu, W. Liu, Y. Kou, X. Yang, Z. Ju and W. Liu, *Inorg. Chem. Front.*, 2022, **9**, 4065–4074.
122 C. M. R. Almeida, J. M. C. S. Magalhaes, M. F. Barroso and L. Duraes, *J. Mater. Chem. C*, 2022, **10**, 15263–15276.
123 H.-Y. Li, H. Xu, S.-Q. Zang and T. C. W. Mak, *Chem. Commun.*, 2016, **52**, 525–528.
124 Z. Li, G. Wang, Y. Ye, B. Li, H. Li and B. Chen, *Angew. Chem., Int. Ed.*, 2019, **58**, 18025–18031.
125 H.-S. Li, S.-H. Xing, Y. Xiao, C. Wang, Q.-L. Guan, F.-Y. Bai, Y.-H. Xing and F. Xu, *Chem. – Eur. J.*, 2022, **29**, e202202810.
126 W.-B. Chen, Y.-C. Chen, G.-Z. Huang, J.-L. Liu, J.-H. Jia and M.-L. Tong, *Chem. Commun.*, 2018, **54**, 10886–10889.
127 O. Cador, B. Le Guennic and F. Pointillart, *Inorg. Chem. Front.*, 2019, **6**, 3398–3417.
128 M. Hojorat, H. Al Sabea, L. Norel, K. Bernot, T. Roisnel, F. Gendron, B. Le Guennic, E. Trzop, E. Collet, J. R. Long and S. Rigaut, *J. Am. Chem. Soc.*, 2020, **142**, 931–936.
129 Y.-J. Ma, J.-X. Hu, S.-D. Han, J. Pan, J.-H. Li and G.-M. Wang, *J. Am. Chem. Soc.*, 2020, **142**, 2682–2689.
130 Y.-X. Wang, Y. Ma, J.-S. Wang, Y. Yang, Y.-N. Guo, Y.-Q. Zhang, K.-J. Jin, Y. Sun and P. Cheng, *Adv. Sci.*, 2022, **9**, 2202979(7).
131 J.-K. Ou-Yang, N. Saleh, G. Fernandez Garcia, L. Norel, F. Pointillart, T. Guizouarn, O. Cador, F. Totti, L. Ouahab, J. Crassous and B. Le Guennic, *Chem. Commun.*, 2016, **52**, 14474–14477.
132 Z. Zhu, C. Zhao, T. Feng, X. Liu, X. Ying, X.-L. Li, Y.-Q. Zhang and J. Tang, *J. Am. Chem. Soc.*, 2021, **143**, 10077–10082.

133 M. Atzori, K. Dhbaibi, H. Douib, M. Grasser, V. Dorcet, I. Breslavetz, K. Paillot, O. Cador, G. L. J. A. Rikken, B. Le Guennic, J. Crassous, F. Pointillart and C. Train, *J. Am. Chem. Soc.*, 2021, **143**, 2671–2675.
134 C. Zhao, Z. Zhu, J. Wu, Q. Yang, T. G. Ashebr, X.-L. Li and J. Tang, *Chem. – Eur. J.*, 2023, **29**, e202202896.
135 R. J. Garcia and M. J. Allen, *Eur. J. Inorg. Chem.*, 2012, 4550–4563.
136 D. Y.-M. So and W.-H. Leung, *Coord. Chem. Rev.*, 2017, **340**, 172–197.
137 R. M. Diaz-Rodriguez, D. A. Galico, D. Chartrand, E. A. Suturina and M. Murugesu, *J. Am. Chem. Soc.*, 2022, **144**, 912–921.
138 K. Binnemans, *Coord. Chem. Rev.*, 2015, **295**, 1–45.
139 A. P. S. Samuel, J. Xu and K. N. Raymond, *Inorg. Chem.*, 2009, **48**, 687–698.
140 L. Armelao, S. Quici, F. Barigelletti, G. Accorsi, G. Bottaro, M. Cavazzini and E. Tondello, *Coord. Chem. Rev.*, 2010, **254**, 487–505.
141 T. Xia, Z. Shao, X. Yan, M. Liu, L. Yu, Y. Wan, D. Chang, J. Zhang and D. Zhao, *Chem. Commun.*, 2021, **57**, 3143–3146.
142 L. Ungur, B. Szabo, Z. A. Alothman, A. A. S. Al-Kahtani and L. F. Chibotaru, *Inorg. Chem.*, 2022, **61**(16), 5972–5976.
143 J. Lehr, P. D. Beer, S. Faulkner and J. J. Davis, *Chem. Commun.*, 2014, **50**, 5678–5687.
144 O. Kotova, S. Comby, C. Lincheneaua and T. Gunnlaugsson, *Chem. Sci.*, 2017, **8**, 3419–3426.
145 G.-Q. Jin, Y. Ning, J.-X. Geng, Z.-F. Jiang, Y. Wang and J.-L. Zhang, *Inorg. Chem. Front.*, 2020, **7**, 289–299.
146 A. T. O'Neil, J. A. Harrison and J. A. Kitchen, *Chem. Commun.*, 2021, **57**, 8067–8070.
147 R. A. S. Ferreira, E. Mamontova, A. M. P. Botas, M. Shestakov, J. Vanacken, V. Moshchalkov, Y. Guari, L. F. Chibotaru, D. Luneau, P. S. André, J. Larionova, J. Long and L. D. Carlos, *Adv. Optical Mat.*, 2021, **9**, 2101495.
148 B.-A. N. Willis, D. Schnable, N. D. Schley and G. Ung, *J. Am. Chem. Soc.*, 2022, **144**, 22421–22425.
149 M. Pan, W.-M. Liao, S.-Y. Yin, S.-S. Sun and C.-Y. Su, *Chem. Rev.*, 2018, **118**, 8889–8935.
150 S. V. Eliseeva, E. V. Salerno, B. A. Lopez Bermudez, S. Petoud and V. L. Pecoraro, *J. Am. Chem. Soc.*, 2020, **142**, 16173–16176.
151 N. Kerbellec, D. Kustaryono, V. Haquin, M. Etienne, C. Daiguebonne and O. Guillou, *Inorg. Chem.*, 2009, **48**, 2837–2843.
152 X. Rao, Q. Huang, X. Yang, Y. Cui, Y. Yang, C. Wu, B. Chen and G. Qian, *J. Mater. Chem.*, 2012, **22**, 3210–3214.
153 W. Huang, F. Pan, Y. Liu, S. Huang, Y. Li, J. Yong, Y. Li, A. M. Kirillov and D. Wu, *Inorg. Chem.*, 2017, **56**, 6362–6370.
154 S. Chorazy, K. Kumar, K. Nakabayashi, B. Sieklucka and S. Ohkoshi, *Inorg. Chem.*, 2017, **56**, 5239–5252.
155 J. Rocha, C. D. S. Brites and L. D. Carlos, *Chem. – Eur. J.*, 2016, **22**, 14782–14795.
156 K. Yanagisawa, Y. Kitagawa, T. Nakanishi, T. Seki, K. Fushimi, H. Ito and Y. Hasegawa, *Chem. – Eur. J.*, 2018, **24**, 1956–1961.
157 K. Kumar, S. Chorazy, K. Nakabayashi, H. Sato, B. Sieklucka and S. Ohkoshi, *J. Mater. Chem. C*, 2018, **6**, 8372–8384.
158 X. Z. Wang, X. R. Wang, Y. Y. Liu, J. Z. Huo, Y. Li, Q. Wang, K. Liu and B. Ding, *Ultrason. Sonochem.*, 2019, **59**, 104734.
159 J. Zhou, Q. Liu, W. Feng, Y. Sun and F. Li, *Chem. Rev.*, 2015, **115**, 395–465.
160 R. Rafique, S. K. Kailasa and T. J. Park, *Trends Anal. Chem.*, 2019, **120**, 115646.
161 K. Du, J. Feng, X. Gao and H. Zhang, *Light Sci. Appl.*, 2022, **11**, 222(23).
162 A. Nonat, S. Bahamyirou, A. Lecointre, F. Przybilla, Y. Mely, C. Platas-Iglesias, F. Camerel, O. Jeanin and L. J. Charbonniere, *J. Am. Chem. Soc.*, 2019, **141**, 1568–1576.
163 A. M. Nonat and L. J. Charbonniere, *Coord. Chem. Rev.*, 2020, **409**, 213192(16).
164 Y. Qiao, D.-C. Sergentu, H. Yin, A. V. Zabula, T. Cheisson, A. McSkimming, B. C. Manor, P. J. Carroll, J. M. Anna, J. Autschbach and E. J. Schelter, *J. Am. Chem. Soc.*, 2018, **140**, 4588–4595.
165 P. Fang, L. Wang, G. Zhan, W. Yan, P. Huo, A. Ying, Y. Zhang, Z. Zhao, G. Yu, Y. Huang, S. Gong, L. Duan, Z. Liu, Z. Bian and C. Huang, *ACS Appl. Mater. Interfaces*, 2021, **13**, 45686–45696.
166 M. Runowski, P. Wozny, N. Stopikowska, Q. Guo and S. Lis, *ACS Appl. Mater. Interfaces*, 2019, **11**, 4131–4138.
167 R. Sessoli, D. Gatteschi, A. Caneschi and M. A. Novak, *Nature*, 1993, **365**, 141–143.
168 N. Ishikawa, M. Sugita, T. Ishikawa, S. Koshihara and Y. Kaizu, *J. Am. Chem. Soc.*, 2003, **125**, 8694–8695.
169 A. Zabala-Lekuona, J. M. Seco and E. Colacio, *Coord. Chem. Rev.*, 2021, **441**, 213984.
170 W. Zhang, A. Muhtadi, N. Iwahara, L. Ungur and L. F. Chibotaru, *Angew. Chem., Int. Ed.*, 2020, **59**, 12720–12724.
171 C. A. Gould, K. R. McClain, J. M. Yu, T. J. Groshens, F. Furche, B. G. Harvey and J. R. Long, *J. Am. Soc.*, 2019, **141**, 12967–12973.
172 J. Moutet, J. Schleinitz, L. L. Droitte, M. Tricoire, F. Pointillart, F. Gendron, T. Simler, C. Clavaguéra, B. L. Guennic, O. Cador and G. Nocton, *Angew. Chem., Int. Ed.*, 2021, **60**, 6042–6046.
173 Z. Zhu, M. Guo, X.-L. Li and J. Tang, *Coord. Chem. Rev.*, 2019, **378**, 350–364.
174 S. V. Rao, M. Piccardo and S. Soncini, *Phys. Chem. Chem. Phys.*, 2022, **24**, 9007–9017.
175 Y.-S. Ding, T. Han, Y.-Q. Zhai, D. Reta, N. F. Chilton, R. E. P. Winpenny and Y.-Z. Zheng, *Chem. – Eur. J.*, 2020, **26**, 5893–5902.
176 Y.-C. Chen, J.-L. Liu, W. Wernsdorfer, D. Liu, L. F. Chibotaru, X. M. Chen and M. L. Tong, *Angew. Chem., Int. Ed.*, 2017, **56**, 4996–5000.
177 J. F. Gonzalez, H. Douib, B. Le Guennic, F. Pointillart and O. Cador, *Inorg. Chem.*, 2021, **60**, 540–544.
178 D. N. Woodruff, R. E. P. Winpenny and R. A. Layfield, *Chem. Rev.*, 2013, **113**, 5110–5148.
179 C. A. P. Goodwin, F. Ortu, D. Reta, N. F. Chilton and D. P. Mills, *Nature*, 2017, **548**, 439–442.
180 D. Aravena and E. Ruiz, *Dalton Trans.*, 2020, **49**, 9916–9928.
181 M. Briganti, F. Santanni, L. Tesi, F. Totti, R. Sessoli and A. Lunghi, *J. Am. Chem. Soc.*, 2021, **143**, 13633–13645.
182 S. Mondal and A. Lunghi, *J. Am. Chem. Soc.*, 2022, **144**, 22965–22975.
183 Y. Ma, Y.-Q. Zhai, Q.-C. Luo, Y.-S. Ding and Y.-Z. Zheng, *Angew. Chem., Int. Ed.*, 2022, **61**, e202206022.
184 J.-L. Liu, Y.-C. Chen and M.-L. Tong, *Chem. Soc. Rev.*, 2018, **47**, 2431–2453.
185 Y.-C. Chen, J.-L. Liu, L. Ungur, J. Liu, Q.-W. Li, L.-F. Wang, Z.-P. Ni, L. F. Chibotaru, X.-M. Chen and M.-L. Tong, *J. Am. Chem. Soc.*, 2016, **138**, 2829–2837.
186 P. Zhang, L. Zhang, C. Wang, S. Xue, S.-Y. Lin and J. Tang, *J. Am. Chem. Soc.*, 2014, **136**, 4484–4487.
187 M. Magott, M. Brzozowska, S. Baran, V. Vieru and D. Pinkowicz, *Nat. Commun.*, 2022, **13**, 2014.
188 P. Zhang, M. Perfetti, M. Kern, P. P. Hallmen, L. Ungur, S. Lenz, M. R. Ringenberg, W. Frey, H. Stoll, G. Rauhut and J. van Slageren, *Chem. Sci.*, 2018, **9**, 1221–1230.
189 Y.-C. Chen and M. L. Tong, *Chem. Sci.*, 2022, **13**, 8716–8726.
190 C. A. Gould, K. R. McClain, D. Reta, J. G. C. Kragskow, D. A. Marchiori, E. Lachman, E.-S. Choi, J. G. Analytis, R. D. Britt, N. F. Chilton, B. G. Harvey and J. R. Long, *Science*, 2022, **375**, 198–202.
191 J.-J. Jia, Q.-W. Li, Y.-C. Chen, J.-L. Liu and M.-L. Tong, *Coord. Chem. Rev.*, 2019, **378**, 365–381.
192 Y. Bi, X.-T. Wang, W. Liao, X. Wang, R. Deng, H. Zhang and S. Gao, *Inorg. Chem.*, 2009, **48**, 11743–11747.
193 C.-S. Liu, M. Du, E. C. Sañudo, J. Echeverria, M. Hu, Q. Zhang, L.-M. Zhou and S.-M. Fang, *Dalton Trans.*, 2011, **40**, 9366–9369.
194 J. Long, R. Vallat, R. A. S. Ferreira, L. D. Carlos, F. A. Almeida Paz, Y. Guari and J. Larionova, *Chem. Commun.*, 2012, **48**, 9974–9976.
195 K. Yamashita, R. Miyazaki, Y. Kataoka, T. Nakanishi, Y. Hasegawa, M. Nakano, T. Yamamura and T. Kajiwara, *Dalton Trans.*, 2013, **42**, 1987–1990.
196 K. S. Pedersen, J. Dreiser, H. Weihe, R. Sibille, H. V. Johannesen, M. A. Sorensen, B. E. Nielsen, M. Sigrist, H. Mutka, S. Rols, J. Bendix and S. Piligkos, *Inorg. Chem.*, 2015, **54**, 7600–7606.
197 J.-R. Jiménez, I. F. Díaz-Ortega, E. Ruiz, D. Aravena, S. J. A. Pope, E. Colacio and J. M. Herrera, *Chem. – Eur. J.*, 2016, **22**, 14548–14559.
198 G. Brunet, R. Marin, M.-J. Monk, U. Resch-Genger, D. A. Galico, F. A. Sigoli, E. A. Suturina, E. Hemmer and M. Murugesu, *Chem. Sci.*, 2019, **10**, 6799–6808.
199 D. Errulat, R. Marin, D. A. Galico, K. L. M. Harriman, A. Pialat, B. Gabidullin, F. Iikawa, O. D. D. Couto Jr., J. O. Moilanen,

E. Hemmer, F. A. Sigoli and M. Murugesu, *ACS Cent. Sci.*, 2019, **5**, 1187–1198.
200 M. A. AlDamen, S. Cardona-Serra, J. M. Clemente-Juan, E. Coronado, A. Gaita-Arino, C. Marti-Gastaldo, F. Luis and O. Montero, *Inorg. Chem.*, 2009, **48**, 3467–3479.
201 E. Mamontova, J. Long, R. A. S. Ferreira, A. M. P. Botas, D. Luneau, Y. Guari, L. D. Carlos and J. Larionova, *Magnetochemistry*, 2016, **2**, 41.
202 L. Mandal, S. Biswas, G. Cosquer, Y. Shen and M. Yamashita, *Dalton Trans.*, 2018, **47**, 17493–17499.
203 Z.-L. Wu, J. Dong, W.-Y. Ni, B.-W. Zhang, J.-Z. Cui and B. Zhao, *Inorg. Chem.*, 2015, **54**, 5266–5272.
204 T. Yoshida, D. C. Izougu, D. Iwasawa, S. Ogata, M. Hasegawa, B. K. Breedlove, G. Cosquer, W. Wernsdorfer and M. Yamashita, *Chem. – Eur. J.*, 2017, **23**, 10527–10531.
205 A. Puzan, M. Zychowicz, J. Wang, J. J. Zakrzewski, M. Reczyński, S. Ohkoshi and S. Chorazy, *Dalton Trans.*, 2021, **50**, 16242–16253.
206 D. Rajah, M. C. Pfrunder, B. S. K. Chong, A. R. Ireland, I. M. Etchells and E. G. Moore, *Dalton Trans.*, 2021, **50**, 7400–7408.
207 Y. Xin, J. Wang, M. Zychowicz, J. J. Zakrzewski, K. Nakabayashi, B. Sieklucka, S. Chorazy and S. Ohkoshi, *J. Am. Chem. Soc.*, 2019, **141**, 18211–18220.
208 J.-M. Herrera, S. J. A. Pope, A. J. H. M. Meijer, T. L. Easun, H. Adams, W. Z. Alsindi, X.-Z. Sun, M. W. George, S. Faulkner and M. D. Ward, *J. Am. Chem. Soc.*, 2007, **129**, 11491–11504.
209 E. Chelebaeva, J. Long, J. Larionova, R. A. S. Ferreira, L. D. Carlos, F. A. Almeida Paz, J. B. R. Gomes, A. Trifonov, C. Guerin and Y. Guari, *Inorg. Chem.*, 2012, **51**, 9005–9016.
210 S. Chorazy, M. Wyczesany and B. Sieklucka, *Molecules*, 2017, **22**, 1902.
211 K. Tomono, Y. Tsunobuchi, K. Nakabayashi and S. Ohkoshi, *Inorg. Chem.*, 2010, **49**, 1298–1300.
212 W. von Ammon and G. Gliemann, *J. Chem. Phys.*, 1982, **77**, 2266–2272.
213 S. G. Baca, S. J. A. Pope, H. Adams and M. D. Ward, *Inorg. Chem.*, 2008, **47**, 3736–3747.
214 J. C. Ahern, R. J. Roberts, P. Follansbee, J. McLaughlin, D. B. Leznoff and H. H. Patterson, *Inorg. Chem.*, 2014, **53**, 7571–7579.
215 S. Chorazy, B. Sieklucka and S. Ohkoshi, *Cryst. Growth Des.*, 2016, **16**, 4918–4925.
216 S. Chorazy, J. J. Zakrzewski, J. Wang, S. Ohkoshi and B. Sieklucka, *CrystEngComm*, 2018, **20**, 5695–5706.
217 S. Chorazy, J. J. Zakrzewski, M. Reczyński and B. Sieklucka, *Chem. Commun.*, 2019, **55**, 3057–3060.
218 M. Wyczesany, J. J. Zakrzewski, B. Sieklucka and S. Chorazy, *J. Mater. Chem. C*, 2022, **10**, 12054–12069.
219 J. J. Zakrzewski, B. Sieklucka and S. Chorazy, *Inorg. Chem.*, 2020, **59**, 1393–1404.
220 K. Liu, X. Zhang, X. Meng, W. Shi, P. Cheng and A. K. Powell, *Chem. Soc. Rev.*, 2016, **45**, 2423–2439.
221 M. Wang, X. Meng, F. Song, Y. He, W. Shi, H. Gao, J. Tang and C. Peng, *Chem. Commun.*, 2018, **54**, 10183–10186.
222 J. J. Zakrzewski, K. Kumar, M. Zychowicz, R. Jankowski, M. Wyczesany, B. Sieklucka, S. Ohkoshi and S. Chorazy, *J. Phys. Chem. Lett*, 2021, **12**, 10558–10566.
223 J. Wang, S. Chorazy, K. Nakabayashi, B. Sieklucka and S. Ohkoshi, *J. Mater. Chem. C*, 2018, **6**, 473–481.
224 R. Jankowski, J. J. Zakrzewski, O. Surma, S. Ohkoshi, S. Chorazy and B. Sieklucka, *Inorg. Chem. Front.*, 2019, **6**, 2423–2434.
225 J. J. Zakrzewski, S. Chorazy, K. Nakabayashi, S. Ohkoshi and B. Sieklucka, *Chem. – Eur. J.*, 2019, **25**, 11820–11825.
226 L.-C. Wu, M. B. Nielsen, M. Bremholm, S. R. Madsen, J. Overgaard, M. Newville, Y.-S. Chen and B. B. Iversen, *Chem. Commun.*, 2015, **51**, 8868–8871.
227 M. Reczyński, S. Chorazy, B. Nowicka, B. Sieklucka and S. Ohkoshi, *Inorg. Chem.*, 2017, **56**, 179–185.
228 F. Xiang, S. Chen, Z. Yuan, L. Li, Z. Fan, Z. Yao, C. Liu, S. Xiang and Z. Zhang, *JACS Au*, 2022, **2**, 1043–1053.
229 V. K.-M. Au, D. Wu and V. W.-W. Yam, *J. Am. Chem. Soc.*, 2015, **137**, 4654–4657.
230 H. Lian, X. Cheng, H. Hao, J. Han, M.-T. Lau, Z. Li, Z. Zhou, Q. Dong and W.-Y. Wong, *Chem. Soc. Rev.*, 2022, **51**, 1926–1982.
231 K. Boukheddaden, M. H. Ritti, G. Bouchez, M. Sy, M. M. Dirtu, M. Parlier, J. Linares and Y. Garcia, *J. Phys. Chem. C*, 2018, **122**, 7597–7604.
232 Y. Shu, Q. Ye, T. Dai, Q. Xu and X. Hu, *ACS Sens.*, 2021, **6**, 641–658.
233 Y. Li, S. Zhang and D. Song, *Angew. Chem., Int. Ed.*, 2013, **52**, 710–713.
234 D. Pinkowicz, R. Podgajny, B. Gaweł, W. Nitek, W. Łasocha, M. Oszajca, M. Czapla, M. Makarewicz, M. Bałanda and B. Sieklucka, *Angew. Chem., Int. Ed.*, 2011, **50**, 3973–3977.
235 J.-L. Liu, Y.-C. Chen, Y.-Z. Zheng, W.-Q. Lin, L. Ungur, W. Wernsdorfer, L. F. Chibotaru and M.-L. Tong, *Chem. Sci.*, 2013, **4**, 3310–3316.
236 W. Ahmad, L. Zhang and Y. Zhou, *Photochem. Photobiol. Sci.*, 2014, **13**, 660–670.
237 X. Zhang, V. Vieru, X. Feng, J.-L. Liu, Z. Zhang, B. Na, W. Shi, B.-W. Wang, A. K. Powell, L. F. Chibotaru, S. Gao, P. Cheng and J. R. Long, *Angew. Chem., Int. Ed.*, 2015, **54**, 9861–9865.
238 D.-L. Liu, J.-Y. Wu, G.-Z. Huang, Y.-C. Chen, J.-H. Jia, L. Ungur, L. F. Chibotaru, X.-M. Chen and M.-L. Tong, *Sci. Rep.*, 2015, **5**, 16621.
239 J.-Y. Ge, L. Cui, J. Li, F. Yu, Y. Song, Y.-Q. Zhang, J.-L. Zuo and M. Kurmoo, *Inorg. Chem.*, 2017, **56**, 336–343.
240 S.-S. Sun, Z. Wang, X. W. Wu, J.-H. Zhang, C.-J. Li, S.-Y. Yin, L. Chen, M. Pan and C.-Y. Su, *Chem. – Eur. J.*, 2018, **24**, 10091–10098.
241 M. Liberka, K. Boidachenko, J. J. Zakrzewski, M. Zychowicz, J. Wang, S. Ohkoshi and S. Chorazy, *Magnetochemistry*, 2021, **7**, 79.
242 Q. Zou, T. Shang, X.-D. Huang, Q.-Q. Guo, J.-G. Jia, S.-S. Bao, Y.-Q. Zhang and L.-M. Zheng, *J. Mater. Chem. C*, 2021, **9**, 10749–10758.
243 S. Chorazy, J. J. Zakrzewski, M. Reczyński, K. Nakabayashi, S. Ohkoshi and B. Sieklucka, *J. Mater. Chem. C*, 2019, **7**, 4164–4172.
244 E. V. Salerno, A. N. Carneiro Neto, S. V. Eliseeva, M. A. Hernández-Rodríguez, J. C. Lutter, T. Lathion, J. W. Kampf, S. Petoud, L. D. Carlos and V. L. Pecoraro, *J. Am. Chem. Soc.*, 2022, **144**, 18259–18271.
245 K. Kumar, O. Stefanczyk, S. Chorazy, K. Nakabayashi and S. Ohkoshi, *Angew. Chem., Int. Ed.*, 2022, **61**, e202201265.
246 A. Nexha, J. J. Carvajal, M. C. Pujol, F. Díaza and M. Aguiló, *Nanoscale*, 2021, **13**, 7913–7987.
247 J. Wang, J. J. Zakrzewski, M. Heczko, M. Zychowicz, K. Nakagawa, K. Nakabayashi, B. Sieklucka, S. Chorazy and S. Ohkoshi, *J. Am. Chem. Soc.*, 2020, **142**, 3970–3979.
248 K. Karachousos-Spiliotakopoulos, V. Tangoulis, N. Panagiotou, A. Tasiopoulos, V. Nastopoulos, E. Moreno-Pineda, W. Wernsdorfer, M. Schulze, A. M. P. Botas and L. D. Carlos, *Inorg. Chem.*, 2022, **61**, 18629–18639.
249 J. Corredoira-Vazquez, C. Gonzalez-Barreira, M. Fondo, A. M. Garcia-Deibe, J. Sanmartin-Matalobos, M. A. Hernandez-Rodriguez and L. D. Carlos, *Dalton Trans.*, 2022, **51**, 15593–15600.
250 R. Marin, D. A. Galico, R. Gayfullina, J. O. Moilanen, L. D. Carlos, D. Jaque and M. Murugesu, *J. Mater. Chem. C*, 2022, **10**, 13946–13953.
251 J. Wang, J. J. Zakrzewski, M. Zychowicz, V. Vieru, L. F. Chibotaru, K. Nakabayashi, S. Chorazy and S. Ohkoshi, *Chem. Sci.*, 2021, **12**, 730–741.
252 J.-C. Rybak, L. V. Meyer, J. Wagenhofer, G. Sextl and K. Muller-Buschbaum, *Inorg. Chem.*, 2012, **51**, 13204–13213.
253 K. Kumar, O. Stefanczyk, S. Chorazy, K. Nakabayashi and S. Ohkoshi, *Adv. Optical Mater.*, 2022, **10**, 2201675.
254 L.-Z. Cai, Q.-S. Chen, C.-J. Zhang, P.-X. Li, M.-S. Wang and G.-C. Guo, *J. Am. Chem. Soc.*, 2015, **137**, 10882–10885.
255 X.-D. Huang, G.-H. Wen, S.-S. Bao, J.-G. Jia and L.-M. Zheng, *Chem. Sci.*, 2021, **12**, 929–937.
256 Q. Zhang, S.-D. Han, Q. Li, J.-X. Hu and G.-M. Wang, *Sci. China Mater.*, 2022, **65**, 788–794.
257 X.-D. Huang, Y. Xu, K. Fan, S.-S. Bao, M. Kurmoo and L.-M. Zheng, *Angew. Chem., Int. Ed.*, 2018, **57**, 8577–8581.
258 P.-Y. Liao, Y. Liu, Z.-Y. Ruan, H.-L. Wang, C.-G. Shi, W. Deng, S.-G. Wu, J.-H. Jia and M.-L. Tong, *Inorg. Chem.*, 2023, **62**, 1075–1085.
259 P. Ramaswamy, N. E. Wong and G. K. H. Shimizu, *Chem. Soc. Rev.*, 2014, **43**, 5913–5932.
260 Y. Saito, T. Nojima and Y. Iwasa, *Nat. Rev. Mater.*, 2017, **2**, 16094.
261 L. S. Xie, G. Skorupskii and M. Dinca, *Chem. Rev.*, 2020, **120**, 8536–8580.
262 Q. Pan, Y.-A. Xiong, T.-T. Sha and Y.-M. You, *Mater. Chem. Front*, 2021, **5**, 40–59.
263 Y. Wang, J. Li and D. Viehland, *Mater. Today*, 2014, **17**, 269–275.

264 Y. Hu and S. Ren, *APL Mater.*, 2020, **8**, 080702.
265 G. Cosquer, Y. Shen, M. Almeida and M. Yamashita, *Dalton Trans.*, 2018, **47**, 7616–7627.
266 Y. Shen, G. Cosquer, H. Zhang, B. K. Breedlove, M. Cui and M. Yamashita, *J. Am. Chem. Soc.*, 2021, **143**, 9543–9550.
267 K. Zhang, X. Xie, H. Li, J. Gao, L. Nie, Y. Pan, J. Xie, D. Tian, W. Liu, Q. Fan, H. Su, L. Huang and W. Huang, *Adv. Mater.*, 2017, **29**, 1701804.
268 S. Biswas and P. Neugebauer, *Eur. J. Inorg. Chem.*, 2021, 4610–4618.
269 G.-B. Sun, X.-D. Huang, T. Shang, S. Yan, S.-S. Bao, X.-M. Lu, Y.-Q. Zhang and L.-M. Zheng, *Eur. J. Inorg. Chem.*, 2021, 4207–4215.
270 C. Duan, J. Huang, N. Sullivan and R. O'Hayre, *Appl. Phys. Rev.*, 2020, **7**, 011314.
271 J. Cao, J. Ji and Z. Shao, *Energy Environ. Sci.*, 2022, **15**, 2200–2232.
272 L. He, J. K. Nath, E.-X. Chen, H.-D. Lai, S.-L. Huang and Q. Lin, *Chem. Commun.*, 2019, **55**, 2497–2500.
273 S. Ohkoshi, K. Nakagawa, K. Tomono, K. Imoto, Y. Tsunobuchi and H. Tokoro, *J. Am. Chem. Soc.*, 2010, **132**, 6620–6621.
274 Y. Gao, R. Broersen, W. Hageman, N. Yan, M. C. Mittelmeijer-Hazeleger, G. Rothenberg and S. Tanase, *J. Mater. Chem. A*, 2015, **3**, 22347–22352.
275 M. Reczyński, B. Nowicka, C. Nather, M. Kozieł, K. Nakabayashi, S. Ohkoshi and B. Sieklucka, *Inorg. Chem.*, 2018, **57**, 13415–13422.
276 S.-D. Zhu, J.-J. Hu, L. Dong, H.-R. Wen, S.-J. Liu, Y.-B. Lu and C.-M. Liu, *J. Mater. Chem. C*, 2020, **8**, 16032–16041.
277 X.-N. Zhang, B.-C. Chen, J.-L. Zhang, S.-J. Liu and H.-R. Wen, *Dalton Trans.*, 2022, **51**, 15762–15770.
278 F.-G. Chen, W. Xu, J. Chen, H.-P. Xiao, H.-Y. Wang, Z. Chen and J.-Y. Ge, *Inorg. Chem.*, 2022, **61**, 5388–5396.
279 M. Fiebig, T. Lottermoser, D. Meier and M. Trassin, *Nat. Rev. Mater.*, 2016, **1**, 16046.
280 N. A. Spaldin and R. Ramesh, *Nat. Mater.*, 2019, **18**, 203–212.
281 X.-L. Liu, D. Li, H.-X. Zhao, X.-W. Dong, L.-S. Long and L.-S. Zheng, *Adv. Mater.*, 2021, **33**, 2004542.
282 X.-L. Li, C.-L. Chen, Y.-L. Gao, C.-M. Liu, X.-L. Feng, Y.-H. Gui and S.-M. Fang, *Chem. – Eur. J.*, 2012, **18**, 14632–14637.
283 J. Hao, Y. Zhang and X. Wei, *Angew. Chem., Int. Ed.*, 2011, **50**, 6876–6880.
284 H. Sun, X. Wu, D. F. Peng and K. W. Kwok, *ACS Appl. Mater. Interfaces*, 2017, **9**, 34042–34049.
285 X.-L. Li, C.-L. Chen, H.-P. Xiao, A.-L. Wang, C.-M. Liu, X. Zheng, L.-J. Gao, X.-G. Yang and S.-M. Fang, *Dalton Trans.*, 2013, **42**, 15317–15325.
286 P.-H. Guo, J.-L. Liu, J.-H. Jia, J. Wang, F.-S. Guo, Y.-C. Chen, W.-Q. Lin, J.-D. Leng, D.-H. Bao, X.-D. Zhang, J.-H. Luo and M.-L. Tong, *Chem. – Eur. J.*, 2013, **19**, 8769–8773.
287 P.-H. Guo, Y. Meng, Y.-C. Chen, Q.-W. Li, B.-Y. Wang, J.-D. Leng, D.-H. Bao, J.-H. Jia and M.-L. Tong, *J. Mater. Chem. C*, 2014, **2**, 8858–8864.
288 J. Long, J. Rouquette, J.-M. Thibaud, R. A. S. Ferreira, L. D. Carlos, B. Donnadieu, V. Vieru, L. F. Chibotaru, L. Konczewicz, J. Haines, Y. Guari and J. Larionova, *Angew. Chem., Int. Ed.*, 2015, **54**, 2236–2240.
289 J. Long, M. S. Ivanov, V. A. Khomchenko, E. Mamontova, J.-M. Thibaud, J. Rouquette, M. Beaudhuin, D. Granier, R. A. S. Ferreira, L. D. Carlos, B. Donnadieu, M. S. C. Henriques, J. Am. Paixao, Y. Guari and J. Larionova, *Science*, 2020, **367**, 671–676.
290 D. Pesquera, E. Khestanova, M. Ghidini, S. Zhang, A. P. Rooney, F. Maccherozzi, P. Riego, S. Farokhipoor, J. Kim, X. Moya, M. E. Vickers, N. A. Stelmashenko, S. J. Haigh, S. S. Dhesi and N. D. Mathur, *Nat. Commun.*, 2020, **11**, 3190.
291 R. Gupta and R. K. Kotnala, *J. Mater. Sci.*, 2022, **57**, 12710–12737.
292 A. K. Boudalis, J. Robert and P. Turek, *Chem. – Eur. J.*, 2018, **24**, 14896–14900.
293 X. Liu, B. Wang, X. Huang, X. Dong, Y. Ren, H. Zhao, L. Long and L. Zheng, *J. Am. Chem. Soc.*, 2021, **143**, 5779–5785.
294 C. Train, M. Gruselle and M. Verdaguer, *Chem. Soc. Rev.*, 2011, **40**, 3297–3312.
295 S. Chorazy, R. Podgajny, W. Nitek, T. Fic, E. Gorlich, M. Rams and B. Sieklucka, *Chem. Commun.*, 2013, **49**, 6731–6733.
296 M. Gonidec, E. S. Davies, J. McMaster, D. B. Amabilino and J. Veciana, *J. Am. Chem. Soc.*, 2010, **132**, 1756–1757.
297 B. Han, X. Gao, J. Lv and Z. Tang, *Adv. Mater.*, 2020, **32**, 1801491.
298 M. Atzori, G. L. J. A. Rikken and C. Train, *Chem. – Eur. J.*, 2020, **26**, 9784–9791.
299 M. Atzori, F. Santanni, I. Breslavetz, K. Paillot, A. Caneschi, G. L. J. A. Rikken, R. Sessoli and C. Train, *J. Am. Chem. Soc.*, 2020, **142**, 13908–13916.
300 X. Wang, S.-Q. Wang, J.-N. Chen, J.-H. Jia, C. Wang, K. Paillot, I. Breslavetz, L.-S. Long, L. Zheng, G. L. J. A. Rikken, C. Train, X.-J. Kong and M. Atzori, *J. Am. Chem. Soc.*, 2022, **144**, 8837–8847.
301 J. Chen, C.-L. Hu, F. Kong and J.-G. Mao, *Acc. Chem. Res.*, 2021, **54**, 2775–2783.
302 R. Medishetty, J. K. Zaręba, D. Mayer, M. Samoć and R. A. Fischer, *Chem. Soc. Rev.*, 2017, **46**, 4976–5004.
303 K. Kumar, O. Stefanczyk, K. Nakabayashi, K. Imoto and S. Ohkoshi, *CrystEngComm*, 2019, **21**, 5882–5889.
304 Y. Deng, M. Wang, Y. Zhuang, S. Liu, W. Huang and Q. Zhao, *Light Sci. Appl.*, 2021, **10**, 76.
305 Z.-G. Wu, H.-B. Han, Z.-P. Yan, X.-F. Luo, Y. Wang, Y.-X. Zheng, J.-L. Zuo and Y. Pan, *Adv. Mater.*, 2019, **31**, 1900524.
306 H. Li, H. Li, W. Wang, Y. Tao, S. Wang, Q. Yang, Y. Jiang, C. Zheng, W. Huang and R. Chen, *Angew. Chem., Int. Ed.*, 2020, **59**, 4756–4762.
307 H.-R. Wen, J.-L. Zhang, F.-Y. Liang, K. Yang, S.-J. Liu and C.-M. Liu, *Eur. J. Inorg. Chem.*, 2019, 1406–1412.
308 R. Jankowski, J. J. Zakrzewski, M. Zychowicz, J. Wang, Y. Oki, S. Ohkoshi, S. Chorazy and B. Sieklucka, *J. Mater. Chem. C*, 2021, **9**, 10705–10717.
309 Y. B. Tan, Y. Okayasu, S. Katao, Y. Nishikawa, F. Asanoma, M. Yamada, J. Yuasa and T. Kawai, *J. Am. Chem. Soc.*, 2020, **142**, 17653–17661.
310 N. F. M. Mukthar, N. D. Schley and G. Ung, *J. Am. Chem. Soc.*, 2022, **144**, 6148–6153.
311 B. E. Rez, J. Liu, V. Bereau, C. Duhayon, Y. Horino, T. Suzuki, L. Coolen and J.-P. Sutter, *Inorg. Chem. Front.*, 2020, **7**, 4527–4534.
312 B. Lefeuvre, C. A. Mattei, J. F. Gonzalez, F. Gendron, V. Dorcet, F. Riobe, C. Lalli, B. Le Guennic, O. Cador, O. Maury, S. Guy, A. Bensalah-Ledoux, B. Baguenard and F. Pointillart, *Chem. – Eur. J.*, 2021, **27**, 7362–7366.
313 K. Dhbaibi, M. Grasser, H. Douib, V. Dorcet, O. Cador, N. Vanthuyne, F. Riobe, O. Maury, S. Guy, A. Bensalah-Ledoux, B. Baguenard, G. L. J. A. Rikken, C. Train, B. Le Guennic, M. Atzori, F. Pointillart and J. Crassous, *Angew. Chem., Int. Ed.*, 2022, **62**, e202215558.
314 W. Miao, S. Wang and M. Liu, *Adv. Funct. Mater.*, 2017, **27**, 1701368.
315 J. Zhang, L. Dai, A. M. Webster, W. T. K. Chan, L. E. Mackenzie, R. Pal, S. L. Cobb and G.-L. Law, *Angew. Chem., Int. Ed.*, 2021, **60**, 1004–1010.

